



Article

A New Mechanism of the Selective Photodegradation of Antibiotics in the Catalytic System Containing TiO₂ and the Inorganic Cations

Wojciech Baran, Mateusz Cholewiński, Andrzej Sobczak and Ewa Adamek *

Department of General and Analytical Chemistry, Faculty of Pharmaceutical Sciences in Sosnowiec, Medical University of Silesia in Katowice, Jagiellońska 4, 41-200 Sosnowiec, Poland; wbaran@sum.edu.pl (W.B.); mateochol@tlen.pl (M.C.); asobczak@sum.edu.pl (A.S.)

* Correspondence: eadamek@sum.edu.pl; Tel.: +48-323-641-565

Abstract: The mechanism of sulfisoxazole (SFF) selective removal by photocatalysis in the presence of titanium (IV) oxide (TiO₂) and iron (III) chloride (FeCl₃) was explained and the kinetics and degradation pathways of SFF and other antibiotics were compared. The effects of selected inorganic ions, oxygen conditions, pH, sorption processes and formation of coordination compounds on the photocatalytic process in the presence of TiO₂ were also determined. The Fe³⁺ compounds added to the irradiated sulfonamide (SN) solution underwent surface sorption on TiO₂ particles and act as acceptors of excited electrons. Most likely, the SFF degradation is also intensified by organic radicals or cation organic radicals. These radicals can be initially generated by reaction with electron holes, hydroxyl radicals and as a result of electron transfer mediated by iron ions and then participate in propagation processes. The high sensitivity of SFF to decomposition caused by organic radicals is associated with the steric effect and the high bond polarity of the amide substituent.

Keywords: molecular mechanism; photocatalysis; sulfonamides; free radicals; TiO₂



Citation: Baran, W.; Cholewiński, M.; Sobczak, A.; Adamek, E. A New Mechanism of the Selective Photodegradation of Antibiotics in the Catalytic System Containing TiO₂ and the Inorganic Cations. *Int. J. Mol. Sci.* **2021**, *22*, 8696. <https://doi.org/10.3390/ijms22168696>

Academic Editor: Raphaël Schneider

Received: 27 July 2021

Accepted: 11 August 2021

Published: 13 August 2021

Publisher's Note: MDPI stays neutral with regard to jurisdictional claims in published maps and institutional affiliations.



Copyright: © 2021 by the authors. Licensee MDPI, Basel, Switzerland. This article is an open access article distributed under the terms and conditions of the Creative Commons Attribution (CC BY) license (<https://creativecommons.org/licenses/by/4.0/>).

1. Introduction

Demand for food of animal origin results in an increase in the number of pharmaceuticals used in industrial animal husbandry. As a result, approximately 2/3 of currently produced antibiotics are used in veterinary medicine [1–5]. A significant portion of these drugs enters the environment and can pose a serious risk to biocenosis. Sulfonamides (SNs) cause disorders in the metabolism of soil microorganisms at concentrations 10⁶ times lower than their concentration in manure [6]. Antibiotics, even at sub-inhibitory concentrations, promote the generation of drug resistance in microorganisms in the environment [5–9]. Therefore, these pharmaceuticals can also pose a serious problem to human health [6,10]. Additionally, commonly used biological wastewater treatment methods generate a risk of the transfer of antibiotic resistance genes from active sludge to human pathogens [11].

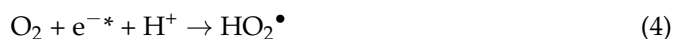
Researchers have high hopes for the use of photocatalytic degradation processes in the presence of TiO₂ to remove xenobiotics from wastewater. The photocatalytic process allows the effective degradation of antibiotics into biologically inactive products and, simultaneously, decomposition of the genetic material present in manure [12–14]. Nowadays, most studies of the photocatalytic degradation of antibiotics have focused on increasing photocatalyst activity and on the use of sunlight [12,15]. Despite the investment of considerable financial resources, however, the problems associated with the application of photocatalytic degradation in wastewater treatment technology have not yet been resolved. The low economic efficiency of the process is unacceptable to food producers. The feasibility of the process is also limited by the level of investment required, the associated operating costs, and its efficiency. Unfortunately, the efficiency of xenobiotics photodegradation in wastewater using simple, low-cost methods is low. One of the reasons for this is the

non-selectivity of the photocatalytic process. Much of the energy is consumed in reactions with other, nontoxic wastewater components that are present in large amounts [16]. A considerable improvement in efficiency would be possible if selective degradation of the selected hazardous component of wastewater could be performed.

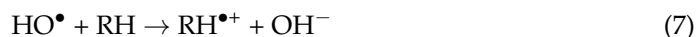
During UV irradiation of TiO₂ particles, high-energy pairs, an excited electron (e^{-*}) and a hole (h⁺) are generated [12,13]:



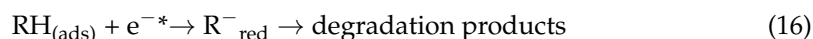
In an aqueous environment saturated with oxygen, the photoinduced pairs initiate the formation of free radicals, e.g., highly active but unstable hydroxyl (HO[•]), more stable but less active superoxide (O₂^{•-}), hydroperoxide (HO₂[•]) and organic (R[•]) radicals [12,13,17]:



Free radicals are very active but react nonselectively. These radicals can react with organic and inorganic compounds or terminate reactions (Equations (6)–(14)):



Moreover, the organic substances adsorbed on the photocatalyst surface can decompose due to direct charge transfer in a manner that does not depend on the presence of free radicals (Equations (15) and (16)):



One of the simple and inexpensive methods that can be used to increase the photocatalytic activity of TiO₂ is the addition of Fe³⁺ salts to the reaction environment. Promising results after the simultaneous use of TiO₂ and FeCl₃ solution were reported by Zhang et al. [18]. This system can intensify the generation of free radicals due to the occurrence of parallel reactions (2) and (17):



An increase in the photodegradation efficiency of the photocatalytic process performed in the presence of Fe³⁺ salts may also be due to an increase in the sorption of anionic reactants on the TiO₂ surface, the formation of coordinate bonds with Fe³⁺ ions

and the binding of e^{-*} . As a result, recombination of the electron-hole pairs is limited (Equation (18)) [18–20]:



According to our previous study, the photodegradation rate of SFF in the presence of $\text{TiO}_2/\text{FeCl}_3$ was even 100 times higher than that of other SN antibiotics [20]. However, the presented hypotheses did not clearly explain why SFF showed high susceptibility to photocatalytic degradation.

The purpose of our paper is to explain the mechanism of selective photodegradation of SFF in wastewater and in combination with its molecular structure. The primary novelty of this research is a new mechanism of the photocatalytic degradation of SFF with the participation of cation radicals and organic radicals, not only hydroxyl radicals. The proposed mechanism is particularly valuable because it is not found in the literature. In the experiments, we compared not only the photodegradation process between various sulfonamides but also between other pharmaceuticals, including antibiotics and anticancer drugs.

In our opinion, in veterinary settings, the use of selected antibiotics that are susceptible to selective photocatalytic degradation in the presence of simple (inexpensive) catalytic systems may be more appropriate than the use of antibiotics whose degradation requires complex (expensive) high-activity systems. This solution can reduce the problem of the low economic efficiency of the photocatalytic process. However, before introducing these antibiotics in veterinary practice, it is necessary to determine the mechanism of their selective susceptibility.

2. Results and Discussion

2.1. Photocatalytic Degradation of Drugs in Wastewater—Screening Tests

Previously published results on SNs photocatalytic degradation [16,20] prompted us to perform screening tests on the susceptibility of various pharmaceuticals (Table S1, Supplementary Materials) to photocatalytic degradation in synthetic wastewater (Table S2, Supplementary Materials) in the presence of a TiO_2 (0.5 g/L)/ FeCl_3 (1.0 mmol/L) mixture. All reactions were conducted at $\text{pH } 3.0 \pm 0.1$ (Section 3.2). The results are shown in Figure 1.

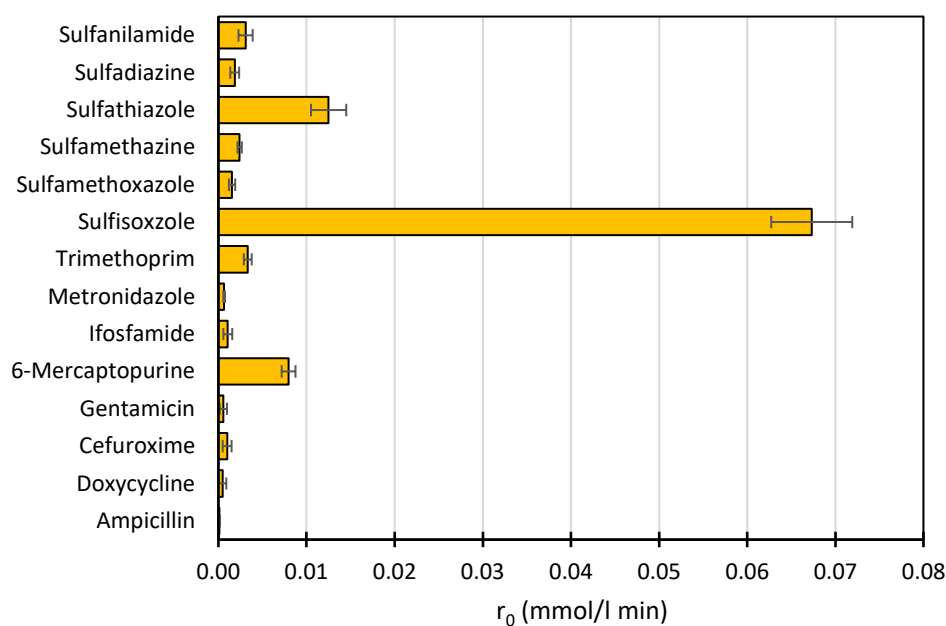


Figure 1. Comparison of the initial photodegradation rates of selected pharmaceuticals in synthetic wastewater in the presence of TiO_2 (0.5 g/L)/ FeCl_3 (1.0 mmol/L).

Under the experimental conditions used, the photodegradation rate of SFF in wastewater was considerably higher than that of the other drugs. At the same time, in contrast

to the other SNs, the degradation rate of SFF in a complex matrix decreased the least compared to the rate in distilled water [20]. This indicates that the studied photocatalytic process can be used for the efficient and selective removal of SFF from wastewater. We performed the experiments described in this paper to determine this.

2.2. Identification of Photocatalytic Degradation Products of the Selected SNs

Aqueous solutions (0.1 mmol/L) of SFF, sulfathiazole (STZ) and sulfanilamide (SAD) were used in the experiments in which we identified photodegradation products. The experiments were performed in the presence of a mixture of TiO₂ (0.5 g/L)/FeCl₃ (1.0 mmol/L) at pH 3.0 ± 0.1. Additionally, products of SFF (0.1 mmol/L) photodegradation conducted in the presence of TiO₂ alone (0.5 g/L) at pH in the range of 4.4–7.5 and in the presence of FeCl₃ alone (1.0 mmol/L) at pH 3.0 ± 0.1 were identified using MSMS technique (Section 3.8). The results are summarized in Table 1. Appropriate chromatograms and MS/MS spectra are included in the Supplementary Materials (Figure S1).

Table 1. Products of the photocatalytic transformation of selected SNs (0.1 mmol/L) conducted in the presence of TiO₂/FeCl₃, TiO₂ and FeCl₃.

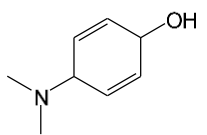
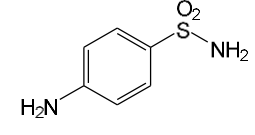
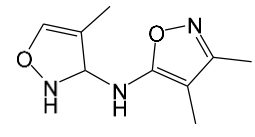
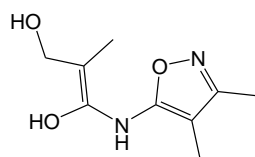
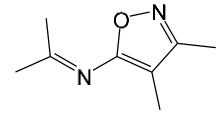
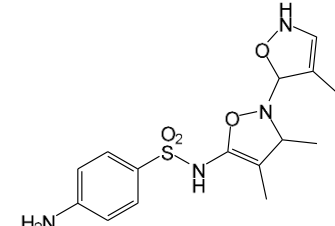
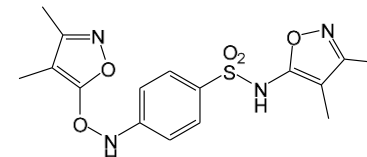
SNs Catalytic System pH	t _R ⁽¹⁾ (min)	Detected Mass M + H ⁺ (Da)	Proposed Molecular Formula	Calculated Mass M + H ⁺ (Da)	Proposed Structural Formula ⁽²⁾
SFF TiO ₂ /FeCl ₃ pH 3.0	0.98	140.1073	C ₈ H ₁₃ NO	140.1075	
	1.37	174.0226 ⁽³⁾	C ₆ H ₈ N ₂ O ₂ S	174.0225	
	1.74	196.1084	C ₉ H ₁₃ N ₃ O ₂	196.1086	
	2.10	199.1078	C ₉ H ₁₄ N ₂ O ₃	199.1083	
	2.45	153.1026	C ₈ H ₁₃ N ₂ O	153.1028	
	3.38	353.1278	C ₁₅ H ₂₁ N ₄ O ₄ S	353.1284	
	5.62	379.1069	C ₁₆ H ₁₈ N ₄ O ₅ S	379.1076	

Table 1. Cont.

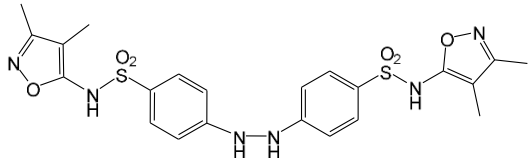
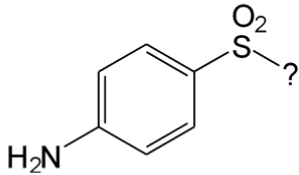
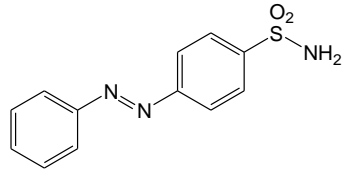
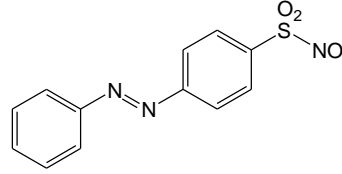
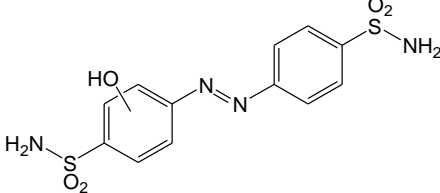
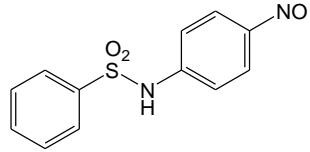
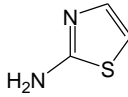
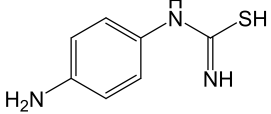
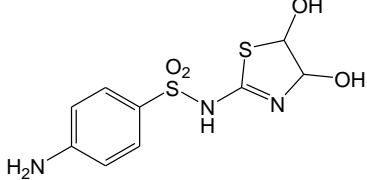
SNs Catalytic System pH	t _R ⁽¹⁾ (min)	Detected Mass M + H ⁺ (Da)	Proposed Molecular Formula	Calculated Mass M + H ⁺ (Da)	Proposed Structural Formula ⁽²⁾
	6.08 6.55	533.1275	C ₂₂ H ₂₄ N ₆ O ₆ S ₂	533.1277	
	6.94	492.1006	C ₂₀ H ₂₁ N ₅ O ₆ S ₂ (3)	492.1011	 (4),(5)
SAD TiO ₂ /FeCl ₃ pH 3.0	2.52 2.58	262.0063	C ₁₂ H ₁₁ N ₃ O ₂ S	262.0061	
	2.64	276.0446	C ₁₂ H ₉ N ₃ O ₃ S	276.0443	
	2.98 3.22	357.0325	C ₁₂ H ₁₂ N ₄ O ₅ S ₂	357.0327	
	3.42	263.0488	C ₁₂ H ₁₀ N ₂ O ₃ S	263.0490	
	3.58 3.66	511.0535 433.0626	? ⁽⁴⁾ C ₁₈ H ₁₆ N ₄ O ₅ S ₂ ?	? 433.0640	? ?
STZ TiO ₂ /FeCl ₃ pH 3.0	0.49	101.0176	C ₃ H ₄ N ₂ S	101.0173	
	1.91	168.0594	C ₇ H ₉ N ₃ S	168.0595	
	2.22	290.0269	C ₉ H ₁₁ N ₃ O ₄ S ₂	290.0269	

Table 1. Cont.

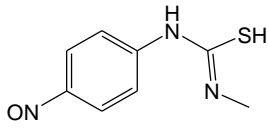
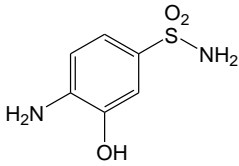
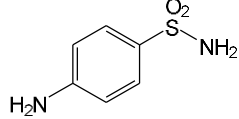
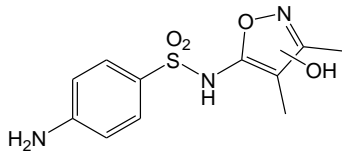
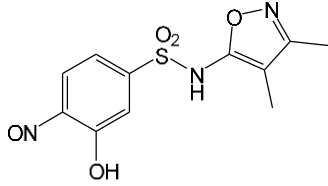
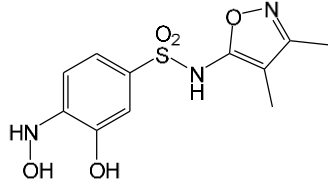
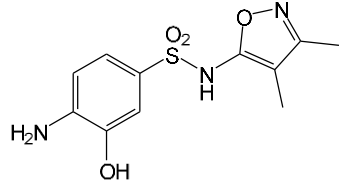
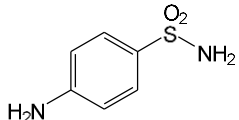
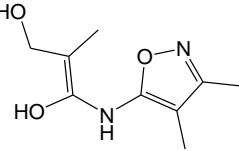
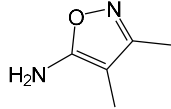
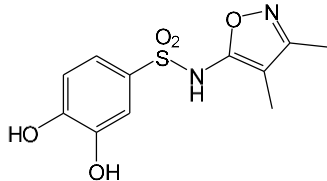
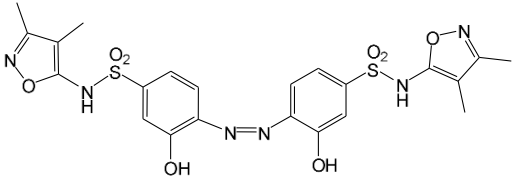
SNs Catalytic System pH	$t_R^{(1)}$ (min)	Detected Mass $M + H^+$ (Da)	Proposed Molecular Formula	Calculated Mass $M + H^+$ (Da)	Proposed Structural Formula ⁽²⁾
SFF TiO ₂ pH 7.5	2.61	196.0541	C ₈ H ₉ N ₃ OS	196.0545	
	3.68	346.0316	C ₁₅ H ₁₁ N ₃ O ₃ S ₂	346.0317	?
	1.29	189.0331	C ₆ H ₈ N ₂ O ₃ S	189.0334	
	1.37	174.0226 ⁽³⁾	C ₆ H ₈ N ₂ O ₂ S	174.0225	
	3.52	284.0705	C ₁₁ H ₁₄ N ₃ O ₄ S	284.0705	
	3.88	298.0497	C ₁₁ H ₁₁ N ₃ O ₅ S	298.0498	
	3.94	300.0652	C ₁₁ H ₁₁ N ₃ O ₅ S	300.0654	
	4.92	284.0705	C ₁₁ H ₁₄ N ₃ O ₄ S	284.0705	
	6.35	387.0756	C ₁₇ H ₁₄ N ₄ O ₅ S ?	387.0763	?
	6.37	392.1025	C ₁₆ H ₁₇ N ₅ O ₅ S ?	392.1029	?
SFF FeCl ₃ pH 3.0	1.37	174.0226 ⁽³⁾	C ₆ H ₈ N ₂ O ₂ S	174.0225	
	2.10	199.1078	C ₉ H ₁₄ N ₂ O ₃	199.1083	

Table 1. Cont.

SNs Catalytic System pH	t _R ⁽¹⁾ (min)	Detected Mass M + H ⁺ (Da)	Proposed Molecular Formula	Calculated Mass M + H ⁺ (Da)	Proposed Structural Formula ⁽²⁾
	2.52	113.0720	C ₅ H ₈ N ₂ O	113.0715	
	5.01	285.0547	C ₁₁ H ₁₂ N ₂ O ₅ S	285.0545	
	5.86	452.0692	C ₁₇ H ₁₈ N ₅ O ₆ S ₂	452.0698	?
	6.80	563.1017	C ₂₂ H ₂₂ N ₆ O ₈ S ₂	563.1019	
	6.97	638.1514	?		?

⁽¹⁾ Retention time on the chromatograms (Figure S1, Supplementary Materials); ⁽²⁾ based on the monoisotopic masses (M + H⁺) and fragmentation spectra; ⁽³⁾ compound identified based on the t_R of the standard; ⁽⁴⁾ (?) structure was not identified; ⁽⁵⁾ a substituent of the sulfonic group was not identified.

Among the photodegradation products of SFF that were formed in the presence of TiO₂/FeCl₃, only two of nine identified products, i.e., C₈H₁₃NO and C₉H₁₄N₂O₃, possessed –OH group(s). These compounds were absent from solutions that had been irradiated for less than 30 s (Figure S1a, Supplementary Materials) and were likely products of subsequent stages of SFF degradation. In turn, a few compounds containing –OH group(s) attached to the aromatic (C₁₂H₁₂N₄O₅S₂) or heterocyclic (C₉H₁₁N₃O₄S₂) ring were identified among the initial products of SAD and STZ photodegradation (Table 1). This may indicate that these SNs reacted with HO• radical (in contrast to SFF) [21].

During the photodegradation of all studied SNs in the presence of TiO₂/FeCl₃, many products with molecular masses significantly higher than the masses of the parent compounds were formed. These compounds likely resulted from the condensation of SNs and/or their degradation products and might possess azo bonds.

A condensation product of two C₁₁H₁₄N₃O₄S molecules (C₂₂H₂₂N₆O₈S₂; Table 1) was also identified after SFF photodegradation in the presence of FeCl₃. Among six identified compounds, four possessed –OH group(s). SAD (C₆H₈N₂O₂S) and 1-amino-3,4-dimethylisoxazole (C₅H₈N₂O) were also identified.

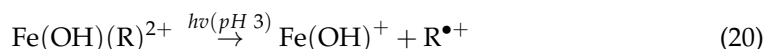
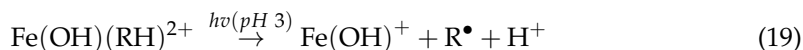
An unusual, extended peak with a retention time of 2.10 min and m/z 199.1078 Da (Figure S1a,b) was observed on the chromatograms after photodegradation of SFF in the presence of a TiO₂/FeCl₃ mixture and after photodegradation of SFF in the presence of FeCl₃ alone. Based on QToF analysis, the compound in this peak may have the formula C₉H₁₄N₂O₃. We suppose that this compound formed as a result of the decomposition of iron complex(es) in the ion source of the mass spectrometer.

After SFF photodegradation in the presence of TiO₂ alone at pH 4.4–7.5, most of the identified products had –OH group(s) attached directly to the original SN structure or to its nitrosyl derivative. An SFF structure with an –OH group attached to the benzene ring (C₁₁H₁₄N₃O₄S, Table 1) was identified in the first sample taken after 1 min of irradiation. In contrast to reactions performed in the presence of TiO₂/FeCl₃ and FeCl₃, condensation products of SFF were not identified when the reactions were performed in the presence of TiO₂ at pH 4.4–7.5 (Table 1). However, these compounds were observed during the photo-

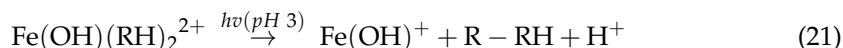
catalytic degradation of SNs with TiO₂ at lower pH (results not shown). The formation of these condensation compounds is also possible during the Fenton process [17].

The abovementioned results confirm that the mechanisms of SNs photodegradation conducted in the presence of various catalytic systems differed. We suspect that when TiO₂ or FeCl₃ was used as the catalyst, the main pathway of SFF photodegradation proceeded through the HO• radical. This radical can also initiate the degradation of SAD and STZ in the presence of a TiO₂/FeCl₃ mixture. No evidence of the involvement of HO• radicals in the initiation of SFF degradation in this catalyst system was found.

According to Ge et al. [21], degradation of five-membered SNs can proceed as a result of direct photolysis without the participation of HO• radicals. SFF is more susceptible than other SNs to photolysis initiated by UVC radiation [22]. However, under direct photolysis, the degradation products of SFF should be primarily sulfanilic acid and 5-amino-3,4-dimethylisoxazole [21]. In our experiments, those compounds were not detected in the solution after the photocatalytic degradation of SFF with a TiO₂/FeCl₃ mixture. Moreover, SFF does not differ from other SNs in its rate of photodegradation initiated by UVA radiation with TiO₂ [20]. The presence of condensation products in solutions after photocatalysis suggests that the transformation of SNs may be initiated not through HO• radicals but through organic radicals or cation radicals (Equations (13) and (14)). These radicals, which form according to Equations (5)–(7), can diffuse into the bulk solution and react with SNs that are not adsorbed on the catalyst surface. Radicals formed as a result of irradiation of coordination compounds of Fe³⁺ (Equations (19) and (20)) may also affect the intensification of the discussed process [17,23].



The condensation products can also form as a result of charge transfer reactions (Equation (21)).



Epoxides, which indicate the peroxides formed during the reaction, were not identified among the products analyzed [24].

SFF degradation products, e.g., SAD and its dimers and dimethylisoxazole adducts, exhibit a breakdown of the bond between the amide nitrogen and the heterocyclic substituent. This was reported in 1973 by Manzo et al. [25]. In turn, 1-amino-3,4-dimethylisoxazole, which formed in the presence of FeCl₃, could be the product of hydrolysis of the amide group in SFF. In this case, sulfanilic acid should also form. This compound is often found among the products of photocatalytic degradation of other SNs [26–28]. However, sulfanilic acid was not identified in the solutions after SFF degradation.

Based on the products we identified, we suspect that HO• radicals do not participate in the main pathway of SFF photodegradation in the presence of TiO₂/FeCl₃. Most likely, due to the acidic reaction environment, propagation reactions involving organic radicals and/or cation radicals are of key importance for SFF photodegradation. A parallel, light-initiated charge transfer within the SFF-iron complex is also possible.

2.3. Study of the Kinetics of Photocatalytic Degradation of SFF in the Presence of a TiO₂/FeCl₃ Mixture

Preliminary studies have confirmed that the SFF degradation reaction that occurs in the presence of TiO₂/FeCl₃ proceeds according to pseudo-first-order kinetics and that its initiating factor is UVA radiation. In the dark, SFF did not undergo degradation after adsorption equilibrium was established (Figure S2, Supplementary Materials).

2.3.1. pH Effect

The pH of the irradiated solution has a strong effect on the kinetics of photocatalytic degradation of SNs in the presence of $\text{TiO}_2/\text{FeCl}_3$ [29]. The relationship between the photocatalytic degradation rate of SFF (0.1 mmol/L) and pH in the range 1 to 6 is shown in Figure 2. The process was conducted in the presence of a TiO_2 suspension (0.5 g/L) and FeCl_3 solution (1.0 mmol/L). Detailed information on the results obtained over a wider pH range is provided in Figure S3 (Supplementary Materials).

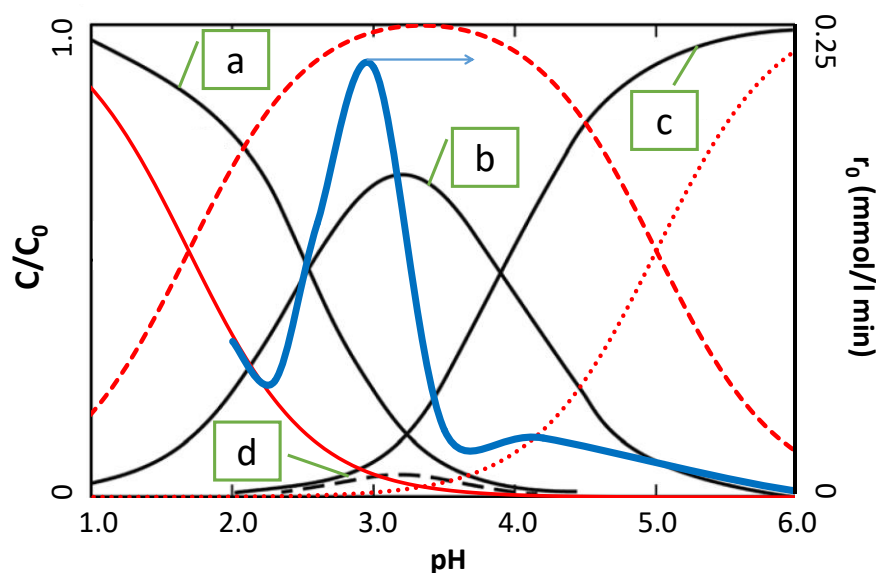


Figure 2. Effect of the pH of the aqueous solution on various parameters of the photocatalytic transformation of SFF (0.1 mmol/L) in the presence of a mixture of TiO_2 (0.5 g/L) and FeCl_3 (1.0 mmol/L): rate of photodegradation of SFF (blue line); concentration of the cationic form of SFF (solid red line); concentration of the neutral form of SFF (red dashed line); concentration of the anionic form of SFF (red dotted line); (a) concentration of $[\text{Fe}(\text{H}_2\text{O})_6]^{3+}$ ions; (b) concentration of $[\text{Fe}(\text{H}_2\text{O})_5(\text{OH})]^{2+}$ ions; (c) concentration of $[\text{Fe}(\text{H}_2\text{O})_4(\text{OH})_2]^+$ ions; (d) concentration of $[\text{Fe}_2(\text{H}_2\text{O})_8(\text{OH})_2]^{4+}$ ions.

The optimal pH for SFF photodegradation in the presence of $\text{TiO}_2/\text{FeCl}_3$ was observed to fall within a narrow range around pH~3. Increasing or decreasing the pH resulted in strong inhibition of the reaction. Analogous results were described for other reactants degraded in the presence of $\text{TiO}_2/\text{Fe}^{3+}$ [18,20,30–34]. According to the majority of researchers, this effect is likely related to the presence of photochemically active $\text{Fe}(\text{OH})^{2+}$ ions in the Fe^{3+} —salt solution at pH~3. The significant inhibition of the reaction at higher pH can be explained by the further hydrolysis of iron compounds to inactive $\text{Fe}(\text{OH})^{2+}$ ions, followed by the formation of $\text{Fe}(\text{OH})_3$ and $\text{Fe}(\text{OH})_4^-$ [35]. These compounds could block access of SFF to the TiO_2 surface and hinder the formation of complex compounds that may participate in the photocatalytic process.

The addition of Fe^{3+} salt to the photocatalyst suspension can also affect the conditions under which reactant sorption occurs. At pH~3, the molar fraction (X) of the molecular form of SFF was higher than that of the other SNs studied (Table S3, Supplementary Materials). In our opinion, the optimal conditions that favor the cumulation of neutral SFF molecules at a positively charged surface of the $\text{TiO}_2/\text{FeCl}_3$ system occur at this pH. Under these conditions, the anionic forms of SNs should be adsorbed to a much greater extent; therefore, the photodegradation rates of SAD ($X_{S^-} = 0.224$) and STZ ($X_{S^-} = 0.142$) should be much higher than that of SFF ($X_{S^-} = 0.056$). In fact, the photodegradation rate of SFF was the highest. This suggests that the anionic forms of SNs are less susceptible to photodegradation than neutral particles. This conclusion may be of key importance when considering the reaction rate.

2.3.2. Effect of the Initial Concentration of SFF

The relationship between the initial concentration of SFF (0.01–0.20 mmol/L) and its photodegradation rate is shown in Figure 3. The reaction was performed at pH 3.0 ± 0.1 in the presence of a TiO_2 (0.5 g/L)/ FeCl_3 (1.0 mmol/L) mixture.

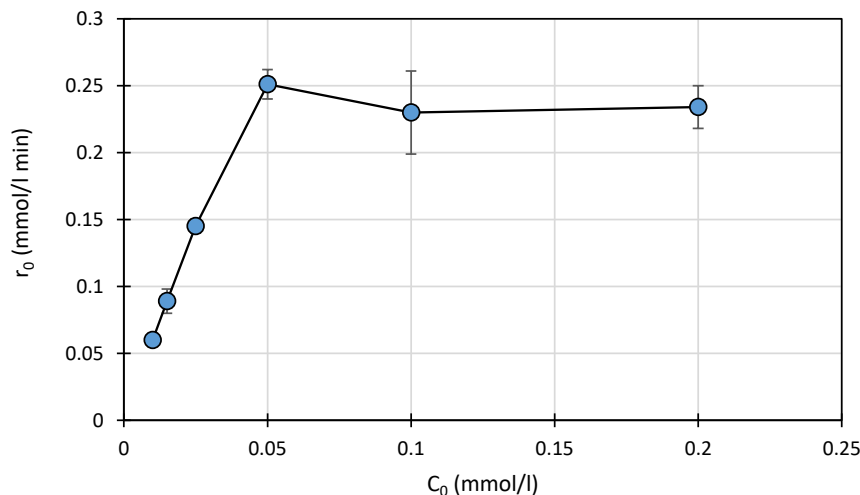


Figure 3. Effect of the initial SFF concentration on the photodegradation rate in the presence of a mixture of TiO_2 (0.5 g/L) and FeCl_3 (1.0 mmol/L) at pH 3.0 ± 0.1 .

Increasing the initial SFF concentration from 0.01 to 0.05 mmol/L resulted in a linear increase in the reaction rate (Figure 3). However, increasing the SFF concentration beyond 0.05 mmol/L did not increase the initial degradation rate, and the reactant concentration hardly affected the r_0 value.

The relationship between the degree of adsorption and the initial SFF concentration showed a similar pattern (Figure S4, Supplementary Materials). An increase in adsorption from ~1.5 to ~5% was observed only when the initial SFF concentration was ≤ 0.05 mmol/L. The reactant molecules most likely occupied the available active sites on the catalyst surface until saturation occurred at a concentration of 0.05 mmol/L. This indicates that, according to the Langmuir–Hinshelwood theory (L–H), the reaction rate is limited by the number of active sites on the photocatalyst [36–38].

This assumption is confirmed by the linearity of the relationship $1/r_0 = f(1/C_0)$ for SFF at concentrations < 0.05 mmol/L (Figure 4). Based on these results, we assume that sorption processes can be of significant importance and may be a factor that limits the photodegradation rate of SFF in the presence of $\text{TiO}_2/\text{FeCl}_3$.

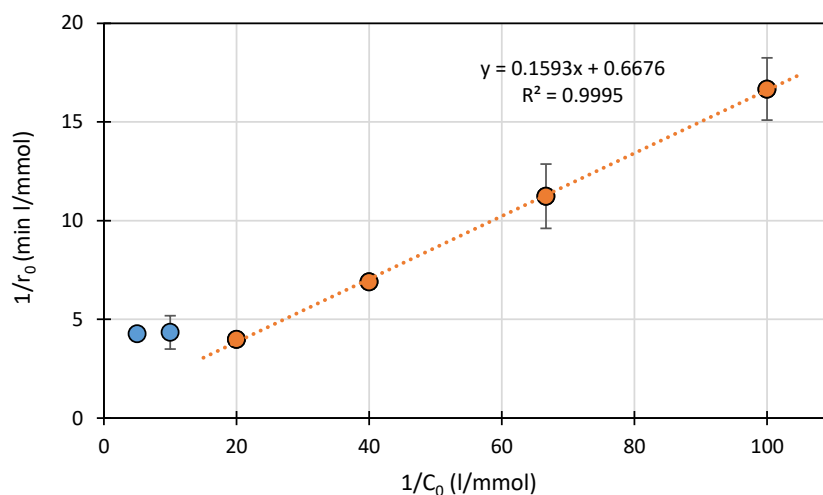


Figure 4. Plot of $1/r_0$ as a function of $1/C_0$ for SFF photodegradation in the presence of $\text{TiO}_2/\text{FeCl}_3$.

2.3.3. Effect of TiO₂ Amount

The effect of TiO₂ amount (0–1 g/L) on the initial rate of photocatalytic degradation of SFF (0.1 mmol/L) in the presence of FeCl₃ (1.0 mmol/L) at pH 3.0 ± 0.1 is shown in Figure 5.

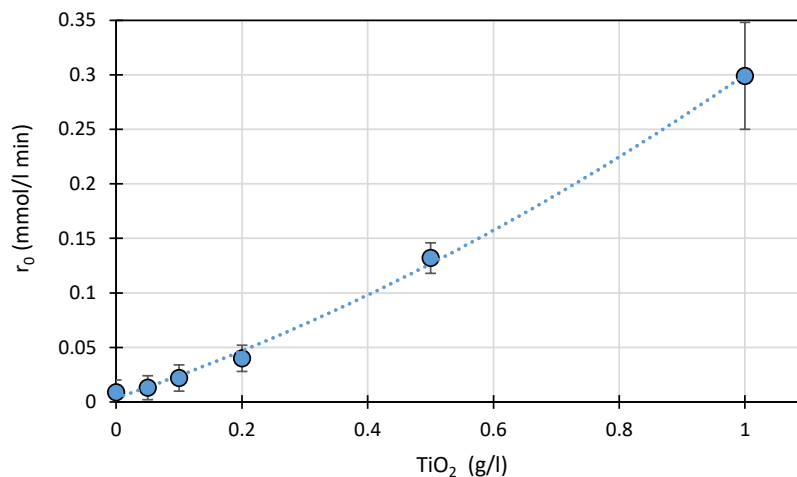


Figure 5. Effect of the amount of TiO₂ present on the photodegradation rate of SFF (0.1 mmol/L) in the presence of FeCl₃ (1.0 mmol/L) at pH 3.0 ± 0.1.

Under these conditions, increasing the concentration of TiO₂ resulted in a monotonic increase in the rate of SFF photodegradation. This result is consistent with the L–H theory because the presence of a larger number of catalyst particles is associated with a greater number of active sites. On the other hand, a 20-fold increase in the amount of TiO₂ present (at a constant FeCl₃ concentration) resulted in only a slight increase in the SFF adsorption rate from ~4 to ~6% (Figure S5, Supplementary Materials).

According to many studies, the initial reaction rate increases as the photocatalyst amount increases up to a certain limit; beyond that limit, it does not accelerate or even slows down [39–41]. This could be due to excessive light scattering by the suspended TiO₂ particles. However, we found no such correlation in our experiments.

The amount of TiO₂ present has a significant effect on the binding of FeCl₃ hydrolysis products (Figure 6). In both the anatase and rutile crystals, the titanium ion (Ti⁴⁺) is surrounded by six oxygen ions (O²⁻) [42]. Therefore, the formation of coordination bonds between oxygen anions from TiO₂ and Fe³⁺ is possible. It is very likely that adsorption of Fe³⁺ compounds on the TiO₂ surface may be important in enhancing photocatalytic processes [18,30].

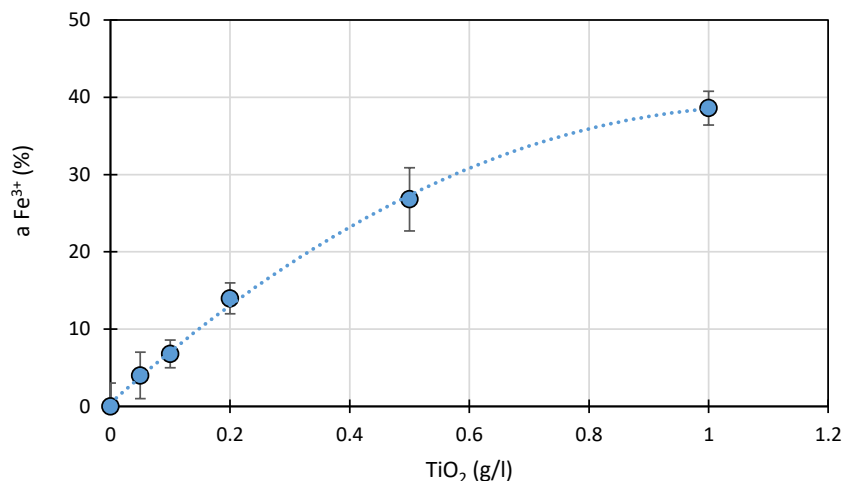


Figure 6. Effect of the amount of TiO₂ present on the sorption (a) of Fe³⁺ compounds from FeCl₃ solution (1.0 mmol/L) at pH 3.0 ± 0.1.

2.3.4. Effect of FeCl₃ Concentration

The relationship between the FeCl₃ concentration (0–2.0 mmol/L) and the rate of photodegradation of SFF (0.1 mmol/L) in the presence of TiO₂ (0.5 g/L) is shown in Figure 7.

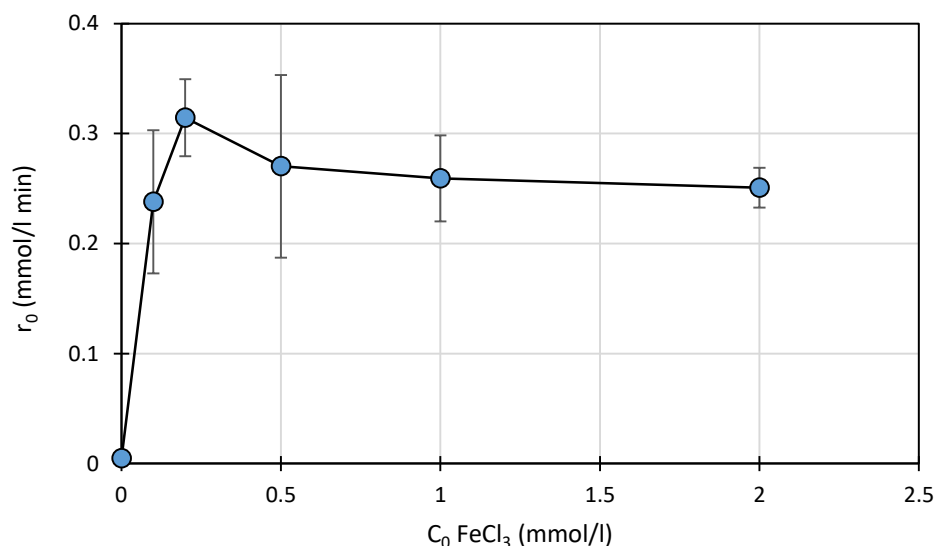


Figure 7. Effect of the initial FeCl₃ concentration on the photodegradation rate of SFF (0.1 mmol/L) in the presence of TiO₂ (0.5 g/L) at pH 3.0 ± 0.1.

SFF exhibited the highest photodegradation rate at a FeCl₃ concentration of 0.2 mmol/L. A further increase in the FeCl₃ concentration to 2.0 mmol/L resulted in a slight decrease in the photodegradation rate. It is possible that a higher Fe-salt concentration reduces the radiant flux that reaches the surface of TiO₂ particles. In addition, polymeric products of hydrolysis (e.g., Fe₂(OH)₂⁴⁺) could form at higher FeCl₃ concentrations at pH 3 [35]. These compounds do not have photocatalytic properties and may block access to active sites in the catalytic system. It cannot also be excluded that FeCl₃ concentration equal to 0.2 mmol/L is optimal from the viewpoint of SFF sorption and desorption of reaction products.

According to certain studies, Cl[−] ions inhibit the photocatalytic process due to their reaction with highly reactive HO• radicals (Equation (22)). Therefore, the supply of HO• radicals in other reactions can be reduced [43–45].



In our opinion, due to their high potential and longer lifetime (Table S4, Supplementary Materials), Cl• radicals may cause an increase in the degradation rates of reactants that are not adsorbed on the TiO₂ surface. However, after SFF photodegradation with TiO₂/FeCl₃, none of the analyzed samples exhibited the presence of chlorine-containing products (Table 1) (theoretically, these products could form under the conditions used here) [45].

2.3.5. Formation of Fe³⁺ Complexes with SNs

The formation of thermodynamically stable coordination compounds of Fe³⁺ with SNs was described previously [17,46,47]. In these compounds, SN can serve as a chelating ligand.

Figure 8 presents the relationship between the FeCl₃ concentration (0.05–2.0 mmol/L) and the amount of bound SFF (0.1 mmol/L) in solutions that had been mixed for 30 min in the dark at pH 3.0 ± 0.1 (Section 3.7). A slight monotonic increase in SFF binding was observed in solutions containing FeCl₃ at a concentration of >0.5 mmol/L. The degree of SFF binding was approximately 10% even when Fe salt was present in 20-fold excess.

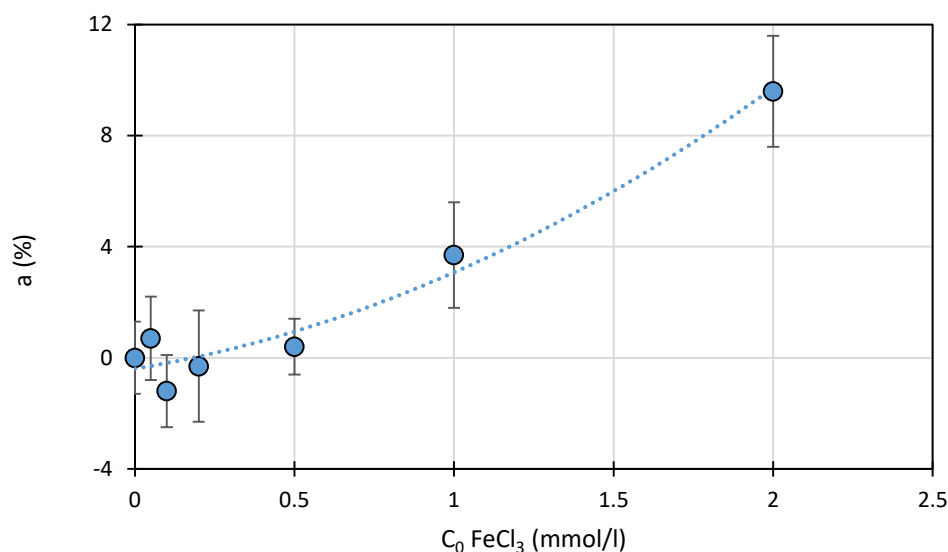


Figure 8. Effect of the initial FeCl_3 concentration on the binding (a) of SFF (1.0 mmol/L) in the dark at $\text{pH } 3.0 \pm 0.1$.

The degree of SFF binding to Fe^{3+} that was significantly lower than expected could be caused by the fact that the resulting $[\text{Fe}^{3+}(\text{SFF})]^{n+}$ complex was soluble (not removed by centrifugation) and, simultaneously, unstable under UPLC analysis.

2.4. Comparison of the Photocatalytic Degradation of SFF with That of Other SNs

To determine the reasons for the higher susceptibility of SFF to photodegradation, the effect of basic parameters of the photocatalytic process on SAD and STZ degradation was studied (Section 3.4). The results are shown in Figure 9.

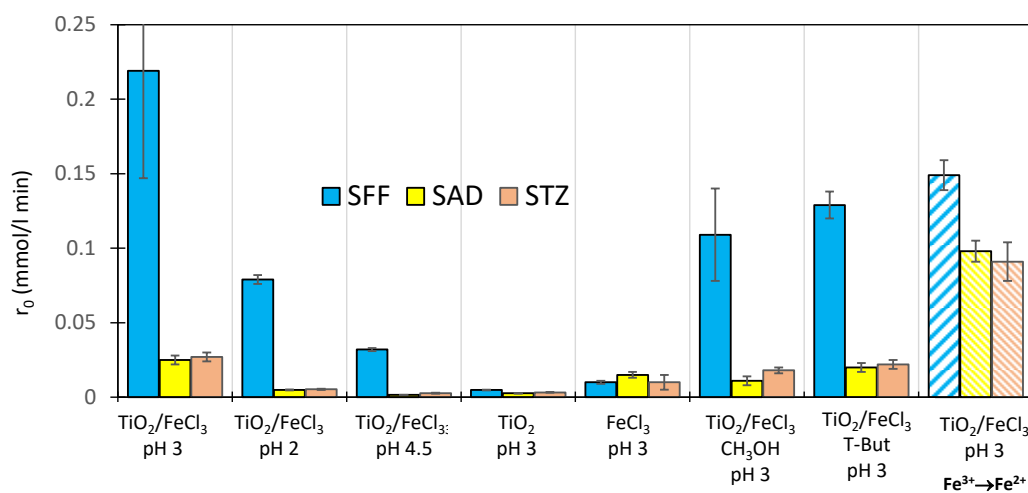


Figure 9. Comparison of the initial rates of photocatalytic degradation of SFF, SAD and STZ (0.1 mmol/L) with the rate of Fe^{3+} reduction in the presence of TiO_2 (0.5 g/L) and/or FeCl_3 (1.0 mmol/L).

With the exception of the reaction performed in the presence of FeCl_3 alone, SFF photodegradation occurred at a significantly higher rate than SAD and STZ photodegradation. In the presence of $\text{TiO}_2/\text{FeCl}_3$ at pH 3, the photodegradation rate of SFF was over eight times higher than that of SAD and STZ. In the presence of TiO_2 alone, the SFF photodegradation rate was two times higher than that of the other SNs, and in the presence of FeCl_3 alone, the photodegradation rate of SAD was the highest. The degradation rates of SFF, SAD and STZ in the $\text{TiO}_2/\text{FeCl}_3$ mixture were ~ 15 , 1.4 and 2 times higher,

respectively than the algebraic sums of the reaction rates determined separately for the processes conducted with TiO_2 and FeCl_3 . It is excluded that the high degradation rate of SFF results from a simple, synergistic generation of HO^\bullet radicals in parallel reactions (Equations (2) and (17)). On the other hand, this synergistic effect may also be important in determining the photodegradation rates of SAD and STZ (Figure 9).

2.5. Total Organic Carbon (TOC) Removal

The dynamics of TOC removal expressed as TOC/TOC_0 are shown in Figure 10.

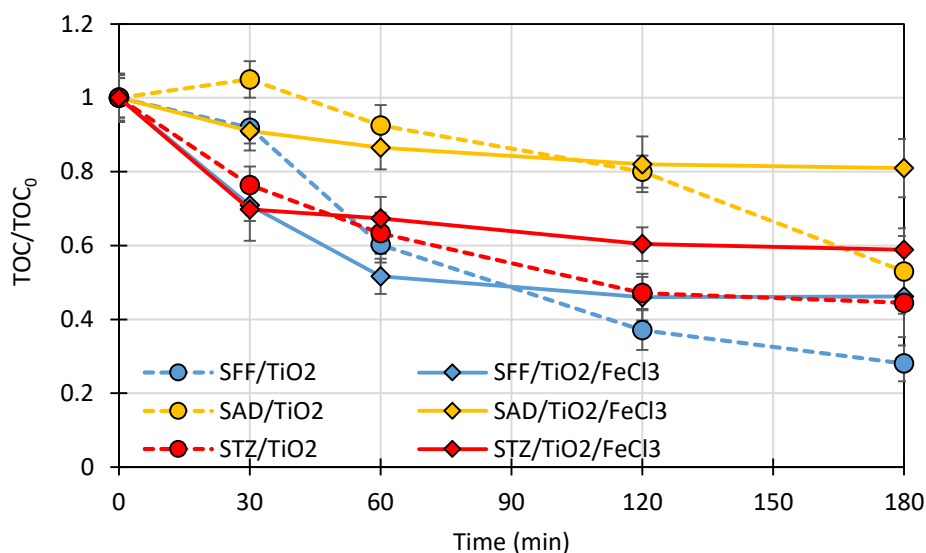


Figure 10. TOC removal during the photocatalytic degradation of SFF, SAD and STZ (0.1 mmol/L) in the presence of TiO_2 (0.5 g/L) and TiO_2 (0.5 g/L)/ FeCl_3 (1.0 mmol/L).

TOC removal is a measure of the mineralization of organic compounds in the sample (Section 3.9). The total photocatalytic mineralization of compounds can be much slower than their photocatalytic degradation. During 180 min experiments, only partial mineralization of the studied SNs was achieved. The addition of FeCl_3 to the SN/ TiO_2 mixture had a negative effect on the process efficiency.

The aim of the photocatalytic removal of antibiotics from the aquatic environment is primarily to remove their antimicrobial activity. It was found that even partial photocatalytic mineralization of antibiotic solutions resulted in the disappearance of their antimicrobial activity [16]. Therefore, a longer UV-irradiation leading to full mineralization of SNS is economically unjustified.

2.6. Kinetics of Fe^{3+} Reduction during SNs Photodegradation in the Presence of a Mixture of $\text{TiO}_2/\text{FeCl}_3$

As mentioned above, during irradiation of solutions containing photoactive Fe^{3+} -compounds, e.g., $\text{Fe}(\text{OH})^{2+}$, Fe^{3+} ions can be reduced to Fe^{2+} ions (Equation (17)). Previous results confirm that the Fe^{2+} concentration increases in a manner that is inversely proportional to the Fe^{3+} concentration during UVA irradiation of the $\text{TiO}_2/\text{FeCl}_3$ mixture [29]. Therefore, an increased supply of HO^\bullet radicals should result from this reduction. Additionally, it cannot be excluded that Fe^{3+} ions can also act as acceptors of photoexcited electrons on the TiO_2 surface (Equation (18)) [30].

Then, the prevention of recombination between e^{-*} and h^+ occurs, and as a consequence, the supply of h^+ in the chain of reactions initiating SN degradation increases. It is possible that both mechanisms have a significant effect on the photodegradation rate of STZ and SAD.

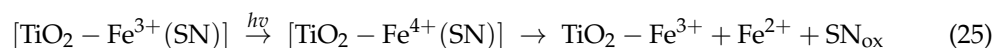
Fe²⁺ ions can be reoxidized to Fe³⁺ using oxidants formed in the irradiated solution (Equations (23) and (24)):



Each of these processes decreases the overall rate of Fe³⁺ reduction but, simultaneously, can also inhibit reactions with h⁺ and HO[•].

The rate of Fe³⁺ reduction depended on the type of SN (Figure 9, dashed bars, and Figure S6, Supplementary Materials). The highest Fe³⁺ reduction rate was observed in samples containing SFF; however, the parallel photodegradation of this drug occurred at a significantly higher rate. In contrast, in the SAD and STZ samples, the rate of reduction of Fe³⁺ was approximately ~3.5–4 times higher than the photodegradation rate (Figure 9).

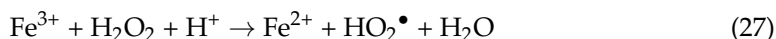
In our opinion, during photodegradation in the presence of TiO₂/FeCl₃, Fe³⁺ ions likely mediate the transfer of electrons from complexed SNs to h⁺. In the transient stage, a complex with Fe⁴⁺ may be formed [17,48,49], and Fe³⁺, Fe²⁺ ions and oxidized SN may be the product of its reduction (Equation (25)):



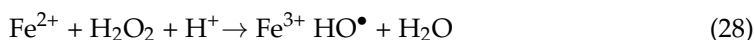
This mechanism does not include the participation of HO[•] radicals in the initiation of SN degradation. Additionally, if the [TiO₂-Fe³⁺(SFF)] complex differs significantly in stability or formation rate from the TiO₂-Fe³⁺ complex formed with other SNs these complexes will significantly differ in the photocatalytic degradation rate. Undoubtedly, the processes leading to the reduction of Fe³⁺ ions (e.g., Equations (17) and (18)) have a positive effect on the rate of SNs photodegradation in the TiO₂/FeCl₃ mixture.

2.7. Fenton-Like Reactions

It is possible that, simultaneously with the photocatalytic process and in the presence of Fe³⁺ salts, Fenton-like reactions proceeded with the participation of formed H₂O₂ molecules (Equations (9), (26) and (27)) [17–51]:



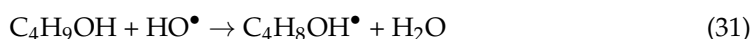
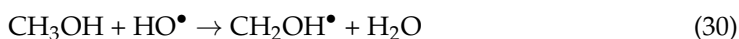
Fe²⁺ ions (Equation (27)) formed in this process can also participate in the generation of HO[•] radicals (Equation (28)):



In this case, the radicals appear in the bulk solution and not on the catalyst surface. They can potentially react with reactant that is not adsorbed on the TiO₂ surface. However, in the Fenton process, SFF does not differ from other SNs in its susceptibility to degradation (Figure S7, Supplementary Materials); therefore, that mechanism is unlikely.

2.8. Photodegradation of SNs in the Presence of a TiO₂/FeCl₃ Mixture with the Addition of Methanol or Tert-Butanol

The addition of excess (100×) methanol and tert-butanol (t-But) has often been used to determine the mechanisms of chemical processes [28,38,44,50]. These compounds, as scavengers, are added to the solutions to inhibit the action of h⁺ or HO[•] radicals (Equations (29)–(31)):



The addition of methanol (10 mmol/L) caused a ~50% decrease in the rate of SFF and SAD photodegradation and a ~30% decrease in the rate of STZ photodegradation. In turn, t-But (10 mmol/L) slowed the photodegradation of these SNs by ~40%, 20% and 20%, respectively (Figure 9). Although the large 100-fold excess of methanol and t-But relative to the SNs, no complete inhibition of the photodegradation of these drugs was found. These results indicate that HO• radicals involved in the initiation of SFF degradation and h⁺ participated in the initiation of SAD degradation. However, it can be concluded that the contribution of these active species was not the most important from the viewpoint of the degradation rate of SNs. In the case of STZ, the supply of h⁺ and HO• has no significant effect on the photodegradation rate. On the other hand, hydroxymethyl (CH₂OH•) and 2-hydroxy-2-methyl-propyl (C₄H₈OH•) radicals also form in these reactions. The possibility that these radicals participate in propagation reactions with SNs cannot be excluded (Equations (8)–(14)).

2.9. Photocatalytic Degradation of SNs in the Presence of a TiO₂/FeCl₃ Mixture under Aerobic and Anaerobic Conditions

Dissolved oxygen is an important reactant in photocatalysis, and it acts mainly as an acceptor of excited electrons (Equations (3), (4) and (12)) [17,42,50]. Additionally, it is a source of HO₂• radicals in processes conducted in acidic environments (Equation (4)). Removal of oxygen from the reaction environment promotes the recombination of the h⁺/e^{-*} pair and consequently inhibits the reactions of SNs with h⁺, HO• and HO₂•. Figure 11 shows the photodegradation rates of the tested SNs (0.1 mmol/L) in the presence of TiO₂ (0.5 g/L) and a mixture of TiO₂/Fe³⁺ salt (1.0 mmol/L) in solutions ventilated with air or argon (Section 3.5). In argon-ventilated solutions, the dissolved oxygen concentration was below 0.5% saturation at 295 K. All reactions were performed at pH 3.0 ± 0.1.

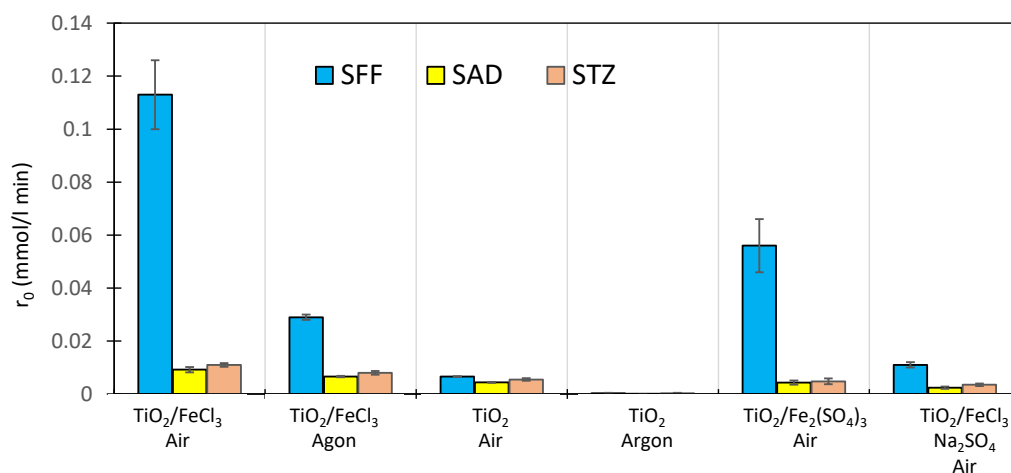


Figure 11. Comparison of the initial rates of photodegradation of SFF, SAD and STZ (0.1 mmol/L) in the presence of TiO₂ (0.5 g/L) and TiO₂ (0.5 g/L)/Fe³⁺ salt (1.0 mmol/L) at pH 3 in samples ventilated with air or argon.

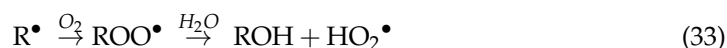
Under anaerobic conditions, the photocatalytic degradation of SNs in the presence of TiO₂ was almost completely inhibited, whereas, in the presence of TiO₂/FeCl₃, it only slowed down. Compared to the reaction with TiO₂/FeCl₃/air, the photodegradation rates of SFF, SAD and STZ decreased by ~80%, 28% and 27%, respectively. These results confirm the hypothesis that in the presence of TiO₂, Fe³⁺ ions act as acceptors of e^{-*} and prevent their recombination with h⁺ [18,19]. In our opinion, this process exerts a decisive influence on the photodegradation rate of SAD and STZ. Moreover, Fe(OH)²⁺ ions adsorbed on the TiO₂ surface can participate in this process by generating an additional quantity of HO• radicals (Equation (32)):



The significant effect of oxygen on the photodegradation rate of SFF in the presence of $\text{TiO}_2/\text{FeCl}_3$ (Figure 10) indicates that the mechanism of degradation of SFF differs from that of SAD and STZ.

In an acidic environment in the presence of oxygen and Fe salts, $(\text{FeO}_2)^{2+}$ ions containing $\text{Fe}^{(\text{IV})}$ may be generated [17,19]. In an aqueous solution, these ions are relatively stable and are active enough that they can even oxidize alkanes [52]. It cannot be excluded that $(\text{FeO}_2)^{2+}$ ions participate in SFF oxidation in the presence of $\text{TiO}_2/\text{FeCl}_3$.

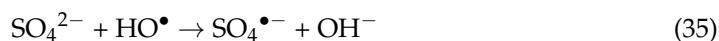
Lack of oxygen in the reaction environment may also inhibit some propagation reactions of organic radicals (Equation (33)).



However, hydroxyl derivatives were formed during this process. As already mentioned, these compounds were not detected in the solution after SFF photodegradation. Therefore, we assume that this process is not a significant determinant of the photodegradation rate of SFF.

2.10. Effect of SO_4^{2-} Ions on the Photocatalytic Degradation of SNs

Photocatalytic degradation of the studied SNs (0.1 mmol/L) in the presence of TiO_2 (0.5 g/L) and $\text{Fe}_2(\text{SO}_4)_3$ (0.5 mol/L) at $\text{pH } 3.0 \pm 0.1$ proceeded two times slowly that was observed in the presence of the $\text{TiO}_2/\text{FeCl}_3$ mixture (Figure 11). However, a stronger inhibitory effect on SNs photodegradation was observed during irradiation of aerated solutions in the presence of $\text{TiO}_2/\text{FeCl}_3/\text{Na}_2\text{SO}_4$ (3 mmol/L). Photodegradation of SNs in the presence of alone $\text{Fe}_2(\text{SO}_4)_3$ proceeded more than three times more slowly than in the presence of alone FeCl_3 [53]. This indicates that SO_4^{2-} ions inhibit the photocatalytic process. SO_4^{2-} ions can react with h^+ and HO^\bullet (Equations (34) and (35)) to form $\text{SO}_4^{\bullet-}$ radicals [45].



They have a high oxidizing potential (Table S4, Supplementary Materials) and can initiate the decomposition of many organic substances, including SNs [45,54–56]. Therefore, we suppose that the abovementioned processes (Equations (37) and (38)) did not slow the degradation of SFF.

The presence of SO_4^{2-} ions in the samples may change the surface charge of the catalyst suspension particles and impede the sorption of neutral reactant particles. It was confirmed that increasing the Na_2SO_4 concentration causes only a slight decrease in the amount of SFF bound by particles in the $\text{TiO}_2/\text{FeCl}_3$ mixture (Figure S8, Supplementary Materials).

The thermodynamic stability of the $[\text{Fe}(\text{SO}_4)]^+$ complex is ten times higher than that of the $[\text{FeCl}]^{2+}$ complex [57]. In addition, the SO_4^{2-} ion can associate with Fe^{3+} ions via two coordination bonds. For these reasons, we assume that SO_4^{2-} ions limit the formation of the $[\text{TiO}_2\text{-Fe}(\text{SFF})]$ complex. In the presence of sulfates (VI), SFF photodegradation was inhibited more strongly than was the photodegradation of other SNs; thus, the reaction rate of SFF is more dependent on the formation of the $[\text{TiO}_2\text{-Fe}(\text{SFF})]$ complex.

2.11. Comparison of the Susceptibilities of the Selected SNs to Photocatalytic Degradation

The particularly high susceptibility of SFF to photodegradation in the presence of $\text{TiO}_2/\text{FeCl}_3$ may be associated with the high polarity of the bond between the amide nitrogen and the heterocyclic substituent ($\text{N}_{\text{amid}}\text{-C}$) [20]. The electroaffinity of the heterocyclic substituent is correlated with the nature of this bond. This parameter also quantitatively affects the dissociation (Table S3, Figure S9, Supplementary Materials).

In the case of two chlorine derivatives of SNs, i.e., sulfachlorpyridazine (SCP) and sulfaclozine (SCL), the concentration of the undissociated form in aqueous solution at pH 3 is similar to that of SFF (Table S3, Supplementary Materials). Therefore, SCP, SCL, SFF,

SAD and STZ were used in experiments intended to assess the effects of $N_{\text{amid}}\text{-C}$ bond polarity and the concentrations of various molecular forms on the SNs photodegradation rate (0.1 mmol/L) in the presence of various catalyst systems (Figure 12).

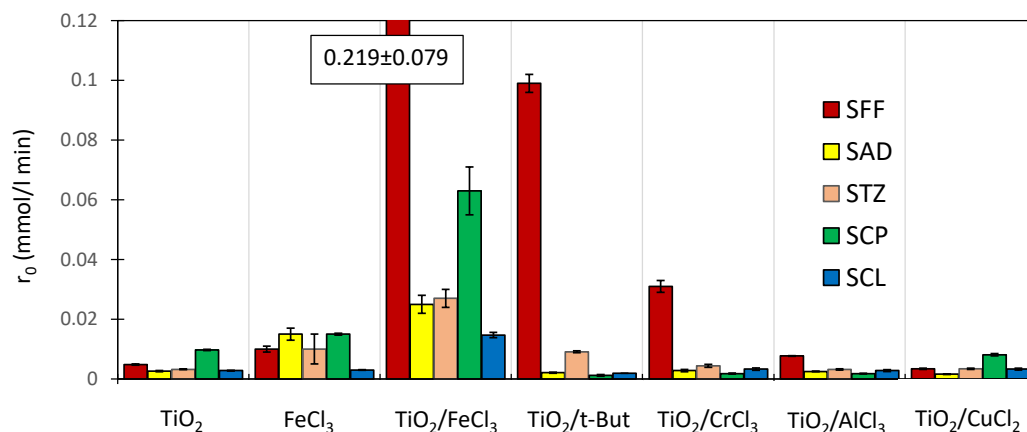


Figure 12. Photodegradation rates of SNs (0.1 mmol/L) in the presence of various catalyst systems at pH 3.0 ± 0.1 .

2.11.1. SNs Photodegradation in the Presence of TiO₂ and/or FeCl₃

In the presence of TiO₂ alone (0.5 g/L) and in the presence of FeCl₃ alone (1.0 mmol/L), SCP underwent the fastest photodegradation. However, the observed differences in the reaction rates of the studied SNs were not high (Figure 12). During the reaction performed in the presence of the TiO₂/FeCl₃ mixture, the photodegradation rates of all studied SNs were higher than the sums of the rates observed in reactions performed separately with TiO₂ or FeCl₃. Similar to SFF, SCP was also degraded at a high rate ($r_0 = 0.063 \pm 0.008$ mmol/L min) in the presence of a TiO₂/FeCl₃ mixture. Surprisingly, the photodegradation of SCL was slower than that of other SNs.

These results indicate that the rate of photodegradation of the studied SNs, with the exception of SCL, in the presence of TiO₂/FeCl₃ increases with an increase in the concentration of the molecular form of SNs in aqueous solution at pH 3 (Figure 13). This result is consistent with our expectation that in this catalytic system, the concentration of the molecular form of SNs is an important determinant of the photodegradation rate.

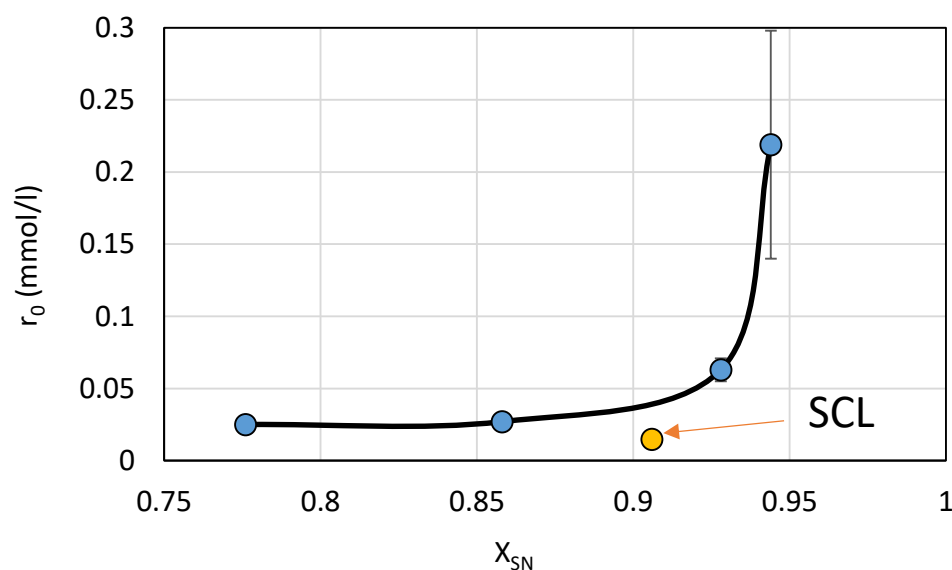


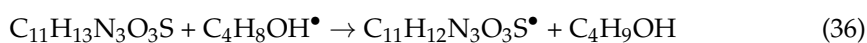
Figure 13. Relationship between the mole fraction of the molecular form of the SN (0.1 mmol/L) in aqueous solution at pH 3 and its photodegradation rate in the presence of TiO₂/FeCl₃.

The relationship between the degradation rate of the studied SNs and the pKa value is linear, with the exception of SCL (Figure S10, Supplementary Materials). The pK_{a2} values and the associated electron affinities of the amide substituents in SCP and SCL are very similar (Table S3, Supplementary Materials). Thus, despite the similarity of the structure of the amide substituent of SCL to that of the amide substituents of the other SNs, its photodegradation rate was much lower than expected (Figure 13). This can probably be attributed to the higher chemical stability of the 6-chloropyrazin-2-yl structure (Table S3, Supplementary Materials) and the higher stability of SCL to degradation in the presence of TiO₂ or FeCl₃ alone. In addition, this structure allows the formation of only one coordination bond involving a lone pair of electrons on the nitrogen atom with Fe³⁺ ion. The two nitrogen atoms in the 3-chloropyridazine ring of the SCP molecule are close to each other, and both can probably coordinate with Fe³⁺. This may affect the higher photodegradation rate of SCP in the presence of FeCl₃ and TiO₂/FeCl₃.

2.11.2. Photodegradation in the Presence of TiO₂/t-But

The addition of t-But (10 mmol/L) increased the photodegradation rate of SFF and STZ at pH 3.0 ± 0.1 in comparison to the experiments performed with TiO₂ alone (Figure 12). This positive effect disappeared with an increase in pH (Figure S11, Supplementary Materials). This may indicate that only neutral SFF and STZ molecules are reactive and can participate in the reaction. In addition, in the presence of TiO₂/t-But, the photodegradation rates of SAD, SCP and SCL decreased.

In the reaction of t-But with HO• radicals (Equation (31)), less active but long-lived C₄H₈OH• radicals formed [58]. The results confirm that, unlike the degradation of other SNs, SFF degradation of neutral SFF molecules can be initiated by less active radicals (Equation (36)).



SFF molecules, whether adsorbed or nonadsorbed, probably react with low-energy radicals generated during the photocatalytic reaction, e.g., with radicals formed in the reaction of SNs and other organic compounds with h⁺ (Equation (5)). These reactive molecules can be generated even from fatty acids, amino acids or sugars during photocatalytic reactions in wastewater. Thus, they probably react with SFF in propagation processes, leading to its degradation. This explains the high photodegradation rate of SFF in wastewater (Section 2.1). In turn, the inhibition of the degradation of other studied SNs (with the exception of STZ) in the presence of t-But indicates that C₄H₈OH• does not initiate their degradation. It is also likely that active molecules generated from wastewater components do not initiate the degradation of other studied drugs (Figure 1). Degradation of the anionic form of SNs occurring at a higher pH (Figure S11, Supplementary Materials) was primarily initiated by HO• radicals [59]. This was confirmed by the presence of hydroxyl derivatives among the products of SFF degradation in the presence of TiO₂ at pH ~7 (Table 1). Therefore, a decrease in the supply of HO• radicals consumed in competitive reactions inhibits photocatalytic degradation at a higher pH.

2.11.3. Photodegradation in the Presence of TiO₂/AlCl₃, TiO₂/CrCl₃ and TiO₂/CuCl₂

The products of partial hydrolysis of Cr³⁺ and Al³⁺ cations and, to a lesser degree, Cu²⁺ affect the surface charge of TiO₂ particles similarly to products of Fe³⁺ ion hydrolysis [60]. The Cr³⁺ ion can also form six coordination bonds, and the Cu²⁺ ion can form four (the complexing properties of Al³⁺ are much lower). Like Fe³⁺, Cr³⁺ cations can serve as electron donors and acceptors, while Cu²⁺ cations can only act as e^{-*} acceptors. For these reasons, photocatalytic degradation of the studied SNs (0.1 mmol/L) in the presence of a mixture of TiO₂ (0.5 g/L) with AlCl₃, CrCl₃ or CuCl₂ salts (1.0 mmol/L) at pH 3.0 ± 0.2 was conducted. The results are presented in Figure 12.

The addition of CrCl₃ caused an increase in the photodegradation rates of SFF and STZ. In the case of SFF, the r₀ value increased almost 6-fold compared to the reaction

conducted in the presence of TiO₂ alone. The addition of AlCl₃ caused a slight increase in the photodegradation rate of SFF only. In other experiments and always after the addition of CuCl₂, a decrease in the photodegradation rate was observed. These results indicate that e^{-*} binding by Cu²⁺ ions did not increase the photodegradation rates of the studied SNs. Moreover, the addition of Al³⁺ salt and the resulting change in the surface charge of TiO₂ (at pH 3) did not significantly increase the photodegradation rate of SNs. In turn, the positive effect of Cr³⁺ ions on SFF photodegradation can indicate that the ability to form multiple coordination bonds with a metal cation that is also redox amphoteric is important.

2.12. Influence of Steric Effect on SNs Binding

Table 1 presents the spatial structures of all of the studied SNs. In the case of STZ, SCP and SKL, the heterocyclic substituent is positioned relative to the benzene ring at an angle of ~90° and the SFF molecule has an approximately linear structure. Therefore, only SFF can bind to the TiO₂/FeCl₃ system via its sulfonamide group (or via heteroatoms of the amide substituent) and via the amino group simultaneously (Figure 14). The resulting bond stress between the amide nitrogen and the heterocyclic substituent most likely facilitates its breaking.

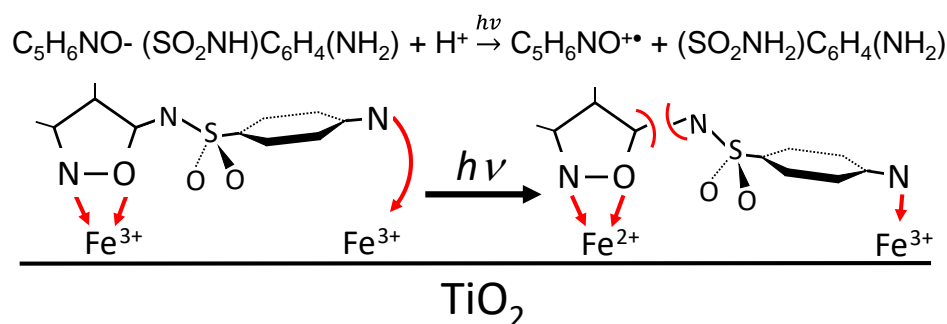


Figure 14. Schematic representation of the binding and light-initiated breaking of SFF molecules in the presence of TiO₂/FeCl₃. The red arrows indicate the direction of mass-transfer or charge-transfer.

This assumption can be confirmed by the presence of SAD and reaction products with the dimethylisoxazole radical in the solution after photocatalytic degradation of SFF (Section 2.2). The other studied SNs cannot simultaneously form coordination bonds with amine nitrogen and heteroatoms of the heterocyclic substituent. The SAD molecule has no heterocyclic substituent, while the spatial arrangement of the benzene ring relative to the heterocyclic substituent in STZ, SCP and SCL prevents the simultaneous formation of these bonds at both ends of the molecules. We assume that this is one of two main reasons for the large differences in the susceptibility of the studied SNs to photocatalytic degradation. However, the presented hypothesis has some limitations. The results of 3D structure analysis using *in silico* methods obtained by various procedures are often divergent (Table S3, Supplementary Materials) [20]. In addition, the hypothesis does not take into account the fact that water molecules can affect the spatial arrangement and the nature of SNs bonds [61]. It is also possible to create multiple bonds between Fe³⁺ and the oxygen in the sulfonamide group [46]. These additional bonds would change the spatial structure of SNs and the way of bonding of SNs molecules on the TiO₂ surface.

2.13. Mechanism of SFF Photodegradation in the Presence of TiO₂/FeCl₃

Figure 15 presents the proposed SFF photodegradation mechanism in the presence of TiO₂/FeCl₃. The studied process can be divided into four stages. Stage I involves the diffusion of reagents to the TiO₂ surface and the formation of coordination bonds with the oxygen atoms at active sites of the photocatalyst. In this way, H₃O⁺, Fe(OH)²⁺ and [Fe(OH)(SFF)]²⁺ cations are adsorbed, while neutral molecules of SFF or O₂ bind to the TiO₂ surface via Fe³⁺ or H₃O⁺ ions. Stage II concerns the processes that occur during irradiation of the reagents in the catalytic system with radiation of λ < 400 nm. Photoexcited h⁺/e^{-*}

pairs form on the TiO₂ surface (Equation (1)) and they initiate charge flow between the catalyst surface and adsorbed compounds (Figure 15, stage III). Additionally, HO• and HO₂• radicals form (Equations (2), (4) and (17)) at stage II. Fe³⁺ cations can also act as e^{-*} acceptors and as an additional source of HO• radicals (Equation (32)). However, we assume that the most important process at this stage is electron transfer from Fe³⁺ to h⁺ and the formation of an active complex containing Fe⁴⁺ (Equation (37)):

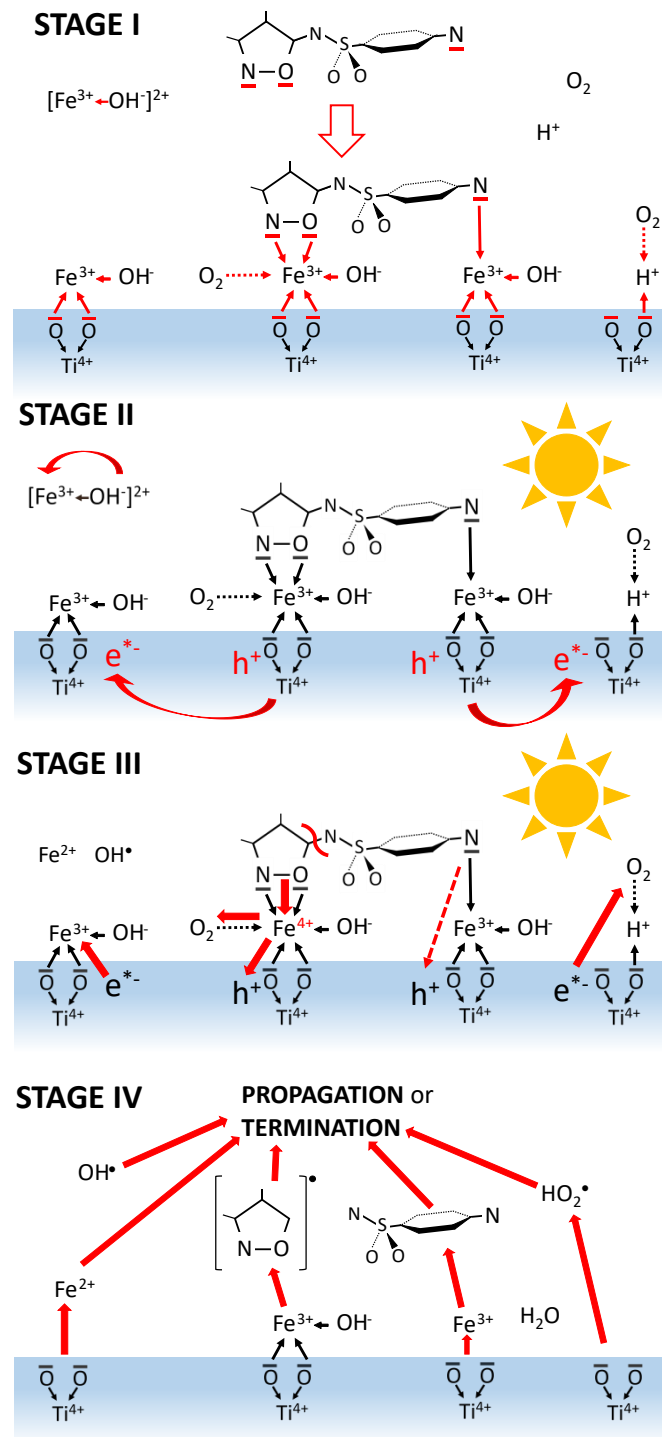


Figure 15. Stages of SFF photocatalytic degradation performed in the presence of TiO₂/FeCl₃. The red arrows indicate the direction of mass-transfer or charge-transfer.

Fe^{4+} can act as an electron acceptor from coordinated SNs molecules due to its high oxidizing potential (Figure 15, stage III). The charge transfer and the energy this process transfers to the SFF molecule can break a bond with the neighboring amide nitrogen, forming the SAD molecule and the $\text{C}_5\text{H}_6\text{NO}^{\bullet+}$ radical. Fe^{2+} cations form as a result of this electron transfer and form much weaker coordination bonds than Fe^{3+} ions. Therefore, the products are released from the TiO_2 surface (Figure 15, stage IV). Desorbed particles, e.g., long-lived free radicals, can participate in propagation and termination reactions with each other, with HO^{\bullet} radicals generated in solution and with not adsorbed molecules of reactants. The final effect of these processes is the total mineralization of organic compounds. It is possible that other processes occur in parallel with degradation in the irradiated mixture, but they do not have a significant effect on the SFF degradation rate in the presence of $\text{TiO}_2/\text{FeCl}_3$ at pH 3.

3. Materials and Methods

3.1. Reagents

The data on the SNs used in the experiments are listed in Table S3, Supplementary Materials. Solid TiO_2 (Aeroxide[®] P25, Degussa, Essen, Germany) was used as the photocatalyst. HCl, NaOH, $\text{FeCl}_3 \cdot 6\text{H}_2\text{O}$, $\text{AlCl}_3 \cdot 6\text{H}_2\text{O}$, $\text{CuCl}_2 \cdot 2\text{H}_2\text{O}$ and Na_2SO_4 (all analytical grade, POCH, Gliwice, Poland), tert-butanol ($\geq 99.5\%$, Sigma-Aldrich, St. Louis, MO, USA), $\text{CrCl}_3 \cdot 6\text{H}_2\text{O}$ ($\geq 98.0\%$, Merck, Darmstadt, Germany) and argon 5.0 (99.999%, Linde Gas, Eggendorf, Austria) were also used in the experiments. In the screening tests, sulfadiazine, sulfamethoxazole, sulfamethoprim, metronidazole, ifosfamide, 6-mercaptopurine, gentamicin, cefuroxime, doxycycline and ampicillin were used. These compounds were added at 0.1 mmol/L to synthetic wastewater prepared according to ISO 9887:1992(E) [62]. Detailed characteristics of the pharmaceuticals and synthetic wastewater components are provided in Tables S1 and S2.

3.2. Screening Tests

A total of 1×10^{-5} mol of each selected pharmaceutical was added to 100 mL of synthetic wastewater (Tables S1 and S2, Supplementary Materials). All of the samples were placed in open glass crystallizers (500 mL, exposed surface: 102 cm²), and solid TiO_2 (50 mg) and FeCl_3 solution (1 mL, 0.1 mol/L) were then added. The pH of the samples was adjusted to 3.0 ± 0.1 with HCl solution (1 mol/L). The pH of the samples was monitored using an HD22569.2 Multimeter (Delta OHM, Caselle di Selvazzano, Italy). After the addition of TiO_2 , all of the operations were conducted under protective (red) light. The samples in the crystallizers were mixed in the dark for 20 min and then irradiated using four fluorescent lamps (Actinic BL W/40, Philips, Amsterdam, The Netherlands). The intensity of radiation at the solution's surface was measured using a quantum photoradiometer DO9721 (Delta OHM, Caselle di Selvazzano, Italy), and the wavelength $\lambda < 400$ nm was approximately 13.6 W/m². During the experiments, the samples had free contact with air, and the temperature was 25 ± 2 °C.

3.3. Studies of the Kinetics of SFF Photocatalytic Degradation

100 mL of SFF solution (0.01–0.5 mmol/L) in redistilled water was placed in open glass crystallizers. Solid TiO_2 (0–1 g/L) and/or an appropriate aliquot of a concentrated FeCl_3 solution was added to this solution. The final concentration of FeCl_3 in the samples ranged from 0.1 to 2.0 mmol/L. If necessary, the pH of the solution was adjusted by adding an appropriate aliquot of HCl or NaOH (1 mol/L) solution. After being stirred in the dark for 20 min, the samples were irradiated (0–60 min) under conditions identical to those described in Section 3.2.

3.4. Comparison of the Photodegradation Kinetics of SFF with Those of Other SNs

100 mL of a solution of each SN (0.1 mmol/L) in redistilled water (Table 1) was placed in open glass crystallizers. Solid TiO_2 (0.5 g/L) and/or 1 mL of a freshly prepared FeCl_3

solution (1.0 mol/L) and/or 1 mL of a solution of a compound that acts as a selective initiator or inhibitor were added to the SNs solutions (Table S5, Supplementary Materials). If necessary, the pH of the solution was adjusted by adding an appropriate aliquot of HCl or NaOH (1 mol/L) solution. After being stirred in the dark for 20 min, the samples were irradiated (0–60 min) under conditions identical to those described in Section 2.2.

3.5. Comparison of the Kinetics of SNs Photodegradation under Aerobic and Anaerobic Conditions

A schematic diagram of the test stand used to irradiate the samples under aerobic and anaerobic conditions is shown in Figure S12 (Supplementary Materials). Open 250 mL beakers containing 150 mL of a solution of SAD, SFF or STZ (0.1 mmol/L) in redistilled water were ventilated for 15 min with compressed air or argon. The concentration of dissolved oxygen in each solution was monitored using a multimeter HD22569.2 outfitted with a probe (D097099S, Delta OHM, Caselle di Selvazzano, Italy). Then, under protective (red) light and without interrupting the gas flow, the selected catalyst system was added to the solutions. After an additional 15 min of ventilation in the dark, the samples were irradiated using four fluorescent lamps (Actinic BL W/40, Philips, Amsterdam, The Netherlands). The radiation intensity measured at the solution's surface was determined to be approximately 13.6 W/m².

3.6. UPLC Analysis

The samples (~2.5 mL) that were collected before and during irradiation were centrifuged immediately (10 min, 4000 RPM). The concentration of SNs in the resulting supernatants was determined by UPLC (ACQUITY UPLC I-Class System, Waters Corp., Milford, MA, USA). An ACQUITY UPLC BEH C18 column (130 Å, 1.7 µm, 2.1 mm × 100 mm) was used at a temperature of 35 °C with sample volumes of 1 µL and 5 µL. Mobile phase A was H₂O (LC-MS grade, LiChrosolv[®], Sigma-Aldrich, St. Louis, MO, USA) containing 0.01% HCOOH (98–100% for LC-MS LiChropur[®], Supelco, Bellefonte, PA, USA), and mobile phase B was CH₃CN (hypergrade for LC-MS LiChrosolv[®], Sigma-Aldrich, St. Louis, MO, USA) containing 0.01% HCOOH. Detailed data on the UPLC analysis are included in Table S6. PDA (λ = 272 nm) and Xevo G2-XS QToF, ESI⁺ detectors (Waters Corp., Milford, MA, USA) were used.

3.7. Fe³⁺ Ions Determination

The Fe³⁺ concentration in the supernatants was determined spectrophotometrically. A total of 1 mL of NH₄SCN solution (20%; analytical grade, POCH, Gliwice, Poland) in redistilled water and 4 mL of HCl solution (0.1 mol/L) were added to 1 mL of supernatant. The absorbance of the samples relative to that of a sample without Fe³⁺ compounds was measured within 5 min (λ = 480 nm, l = 1 cm) using a spectrophotometer (DR 3900, HACH, Düsseldorf, Germany). Method validation was performed using a solution of NH₄Fe(SO₄)₂·12H₂O (analytical grade, POCH, Gliwice, Poland).

3.8. Identification of SNs Photodegradation Products

The products of SNs photodegradation were identified based on a comparison of chromatograms (QToF detector, ESI⁺) of non-irradiated and irradiated samples (Figure S1, Supplementary Materials). The compounds resolved on the chromatograms prior to the irradiation of the samples were not identified. Monoisotope masses (M + H⁺) and fragmentation spectra, which were obtained at fragmentation energies in the range of 10–25 V, were determined for peaks corresponding to the degradation products (Figure S13, Supplementary Materials). Chemical structures were drawn using ChemDraw Std software with the Analysis package (CambridgeSoft). The identification of labile amides and peroxides was not possible due to the type of ion source (ESI⁺) and the type of eluent.

3.9. Total Organic Carbon Analysis

The Total Organic Carbon (TOC) removal in the SNs solutions before and after UV irradiation was performed using the LCK380 cuvette test (HACH LANGE, Düsseldorf, Germany), and the results were read on a DR 3900 spectrophotometer (HACH LANGE, Düsseldorf, Germany).

3.10. Analysis of Results

Graphs of the function $C/C_0 = f(t)$, where C is the reactant concentration after irradiation time (t) and C_0 is the initial reactant concentration, were prepared based on the results of UPLC analysis. The photocatalytic processes that occur in the presence of TiO_2 or $FeCl_3$ are believed to be pseudo-first-order reactions [16,20,36,53]. Therefore, the value of the reaction rate constant (k) was determined from the slope of the linear equation (Equation (38)):

$$\ln(C_0/C) = kt + b \quad (38)$$

where b is the intercept.

The initial reaction rate (r_0) was determined using Equation (38):

$$r_0 = kC_0 \quad (39)$$

The degree of adsorption, binding or removal (a) was determined according to the following equation (Equation (40)):

$$a = 100 \cdot (1 - (C_{eq}/C_0)) \quad (40)$$

where C_{eq} is the equilibrium concentration of SN or Fe^{3+} in the solution after the addition of the catalytic system components (i.e., after adsorption but prior to irradiation).

4. Conclusions

In aqueous solutions, SFF photodegradation in the presence of a $TiO_2/FeCl_3$ mixture was found to occur many times faster than the photodegradation of other pharmaceuticals. The kinetics of this process correlates with the L–H heterogeneous catalysis model, and the optimum pH is sharp at approximately 3.

In the abovementioned catalytic system, $Fe(OH)^{2+}$ ions adsorb onto the TiO_2 surface and simultaneously form complexes with SFF. Neutral SFF molecules coordinated with Fe^{3+} ions are primarily involved in the photocatalytic process. The products of hydrolysis or polymerization of $Fe(OH)^{2+}$ ions inhibit SFF photodegradation.

The amount of SFF adsorbed on $TiO_2/FeCl_3$ at equilibrium is low (<10%), and the resulting complexes are probably labile. The possibility that the SFF photodegradation rate depends on the adsorption rate and not on the adsorption equilibrium cannot be excluded.

The identified products of SFF photodegradation in the presence of $TiO_2/FeCl_3$ are SAD and dimethylisoxazole group adducts. These compounds form as a result of the breakage of the amide bond in the SFF molecule, with the simultaneous formation of dimethylisoxazole radical or cation radicals. Surprisingly, among the SFF photodegradation products, there are no hydroxyl derivatives that are characteristic of analogous reactions conducted in the presence of TiO_2 or $FeCl_3$ and initiated by HO^\bullet radical. The photodegradation rates of all studied SNs in the presence of $TiO_2/FeCl_3$ are much higher than the sums of the photodegradation rates observed in reactions performed in the presence of TiO_2 or $FeCl_3$ individually.

During photodegradation of SNs in the presence of $TiO_2/FeCl_3$, reduction of Fe^{3+} ions occurred in parallel. The rate of this reaction was lower than the SFF photodegradation rate but higher than the photodegradation rates of other SNs.

The factor that determines the rate of SFF photodegradation is probably the charge transfer from the coordinated reactant to h^+ mediated by Fe^{3+} ions. An active complex containing Fe^{4+} and oxygen, as well as long-lived free radicals that participate in the

degradation of subsequent non-adsorbed SFF molecules, can form at this stage. Other reactions, including e^{-*} binding by adsorbed Fe^{3+} compounds, may also occur in parallel.

The presence of other complex-forming Me^{3+} cations that possess oxidation/reduction properties (redox amphoteric) can also, but to a lesser extent, accelerate the SFF photodegradation rate in the presence of TiO_2 . SO_4^{2-} ions limit SFF adsorption to the TiO_2 surface and inhibit photodegradation.

Of the studied SNs, SFF exhibited the highest rate of photodegradation. That effect may be caused by one or more of the following:

- The high bond polarity between the amide nitrogen and the heterocyclic substituents;
- The nearly linear structure of the SFF molecule;
- The specific arrangement of heteroatoms in the heterocyclic moiety, allowing the formation of a chelated complex;
- A high molar fraction of the molecular form in solution at the optimal pH for photocatalytic activity;
- Susceptibility to initiation of the degradation process by low-active, long-lived radicals.

The limitation of SFF photodegradation is the narrow range of the optimal pH value. The improvement of the degradation efficiency of drugs present in large amounts in post-culture wastewater can be achieved by using drugs with a high, selective susceptibility to photocatalytic degradation in animal breeding. The results obtained indicate the feasibility of this solution.

Supplementary Materials: The following are available online at <https://www.mdpi.com/article/10.3390/ijms22168696/s1>. References [63–90] are cited in the supplementary materials.

Author Contributions: W.B. and E.A. conceptualization, designed the experiments, analyzed and discussed the results, writing—review and editing; M.C. carried out the experiments, writing—original draft preparation; A.S. project administration and funding acquisition. All authors have read and agreed to the published version of the manuscript.

Funding: This research was funded by the Medical University of Silesia (Grant number PCN-1-092/K/0/F).

Institutional Review Board Statement: Not applicable.

Informed Consent Statement: Not applicable.

Data Availability Statement: The data presented in this study are available on request from the corresponding author. The data are not publicly available due to very large sizes of chromatographic files.

Conflicts of Interest: The authors declare no conflict of interest.

References

1. Kümmerer, K. Antibiotics in the aquatic environment—A review—Part I. *Chemosphere* **2009**, *75*, 417–434. [[CrossRef](#)]
2. Klein, E.Y.; Van Boeckel, T.P.; Martinez, E.M.; Pant, S.; Gandra, S.; Levin, S.A.; Goossens, H.; Laxminarayan, R. Global increase and geographic convergence in antibiotic consumption between 2000 and 2015. *Proc. Natl. Acad. Sci. USA* **2018**, *115*, E3463–E3470. [[CrossRef](#)]
3. EMA. European Surveillance of Veterinary Antimicrobial Consumption 2019. Sales of Veterinary Antimicrobial Agents in 31 European Countries in 2017. (EMA/294674/2019). Available online: https://www.ema.europa.eu/en/documents/report/sales-veterinary-antimicrobial-agents-31-european-countries-2017_en.pdf (accessed on 7 May 2021).
4. World Health Organization. *WHO Report on Surveillance of Antibiotic Consumption: 2016–2018 Early Implementation*; WHO: Geneva, Switzerland, 2018; Available online: https://www.who.int/medicines/areas/rational_use/oms-amr-amc-report-2016-2018/en/ (accessed on 7 September 2020).
5. Statens Serum Institut National Food Institute, Technical University of Denmark. DANMAP 2019, Use of Antimicrobial Agents and Occurrence of Antimicrobial Resistance in Bacteria from Food Animals, Food and Humans in Denmark. Available online: <https://www.danmap.org> (accessed on 7 May 2021).
6. Baran, W.; Adamek, E.; Ziemiańska, J.; Sobczak, A. Effects of the presence of sulfonamides in the environment and their influence on human health. *J. Hazard. Mater.* **2011**, *196*, 1–15. [[CrossRef](#)] [[PubMed](#)]
7. Ghafur, A.; Vidyalakshmi, P.R.; Murali, A.; Priyadarshini, K.; Thirunarayan, M.A. Emergence of pan-drug resistance amongst gram negative bacteria! The first case series from India. *J. Microbiol. Infect. Dis.* **2014**, *4*, 86–91. [[CrossRef](#)]

8. Giri, P.; Pal, C. Ecotoxicological aspects of pharmaceuticals on aquatic environment. *Am. J. Drug Discov.* **2014**, *1*, 10–24.
9. Spellberg, B.; Bartlett, J.G.; Gilbert, D.N. The Future of Antibiotics and Resistance. *N. Engl. J. Med.* **2013**, *368*, 299–302. [[CrossRef](#)]
10. Walsh, C.; Wencewicz, T. *Antibiotics: Challenges, Mechanisms, Opportunities*; John Wiley & Sons: Washington, DC, USA, 2020.
11. Barancheshme, F.; Munir, M. Development of Antibiotic Resistance in Wastewater Treatment Plants. Antimicrobial Resistance—A Global Threat. In *Antimicrobial Resistance a Global Threat*; Yashwant, K., Ed.; IntechOpen Limited: London, UK, 2019.
12. Humayun, M.; Raziq, F.; Khan, A.; Luo, W. Modification strategies of TiO₂ for potential applications in photocatalysis: A critical review. *Green Chem. Lett. Rev.* **2018**, *11*, 86–102. [[CrossRef](#)]
13. Byrne, C.; Subramanian, G.; Pillai, S.C. Recent advances in photocatalysis for environmental applications. *J. Environ. Chem. Eng.* **2018**, *6*, 3531–3555. [[CrossRef](#)]
14. Tobaldi, D.M.; Piccirillo, C.; Rozman, N.; Pullar, R.C.; Seabra, M.P.; Škapin, A.S.; Labrincha, J.A. Effects of Cu, Zn and Cu-Zn addition on the microstructure and antibacterial and photocatalytic functional properties of Cu-Zn modified TiO₂ nano-heterostructures. *J. Photochem. Photobiol. A Chem.* **2016**, *330*, 44–54. [[CrossRef](#)]
15. Sacco, O.; Vaiano, V.; Rizzo, L.; Sannino, D. Photocatalytic activity of a visible light active structured photocatalyst developed for municipal wastewater treatment. *J. Clean. Prod.* **2018**, *175*, 38–49. [[CrossRef](#)]
16. Adamek, E.; Baran, W.; Ziemiańska, J.; Sobczak, A. Effect of FeCl₃ on sulfonamide removal and reduction of antimicrobial activity of wastewater in a photocatalytic process with TiO₂. *Appl. Catal. B Environ.* **2012**, *126*, 29–38. [[CrossRef](#)]
17. Duca, G. Homogeneous Redox Catalysis with Transition Metal Compounds in Oxide and Peroxide Systems. In *Homogeneous Catalysis with Metal Complexes*; Springer Series in Chemical Physics; Springer: Berlin/Heidelberg, Germany, 2012; Volume 102, pp. 11–121.
18. Zhang, J.; Fu, D.; Gao, H.; Deng, L. Mechanism of enhanced photocatalysis of TiO₂ by Fe³⁺ in suspensions. *Appl. Surf. Sci.* **2011**, *258*, 1294–1299. [[CrossRef](#)]
19. Elghniji, K.; Atyaoui, A.; Livraghi, S.; Boussemli, L.; Giamello, E.; Ksibi, M. Synthesis and characterization of Fe³⁺ doped TiO₂ nanoparticles and films and their performance for photocurrent response under UV illumination. *J. Alloys Compd.* **2012**, *541*, 421–427. [[CrossRef](#)]
20. Adamek, E.; Baran, W.; Sobczak, A. Effect of FeCl₃ on the photocatalytic processes initiated by UVa and vis light in the presence of TiO₂-P25. *Appl. Catal. B Environ.* **2015**, *172–173*, 136–144. [[CrossRef](#)]
21. Ge, P.; Yu, H.; Chen, J.; Qu, J.; Luo, Y. Photolysis mechanism of sulfonamide moiety in five-membered sulfonamides: A DFT study. *Chemosphere* **2018**, *197*, 569–575. [[CrossRef](#)]
22. Lian, J.; Qiang, Z.; Li, M.; Bolton, J.R.; Qu, J. UV photolysis kinetics of sulfonamides in aqueous solution based on optimized fluence quantification. *Water Res.* **2015**, *75*, 43–50. [[CrossRef](#)]
23. Prajapat, G.; Gupta, R.; Bhojak, N. Microwave Assisted Synthesis, Structural Characterization, Thermal Analysis and Antibacterial Studies of Fe(III), Ni(II) and Cu(II) Complexes of Sulfanilamide. *Orient. J. Chem.* **2019**, *35*, 308–317. [[CrossRef](#)]
24. Kanavouras, A.; Hernandez-Munoz, P.; Coutelieis, F.A. Packaging of Olive Oil: Quality Issues and Shelf Life Predictions. *Food Rev. Int.* **2006**, *22*, 381–404. [[CrossRef](#)]
25. Manzo, R.H.; de Bertorello, M.M. Isoxamles II: Kinetics and Mechanism of Degradation of Sulfoxazole in Moderately Concentrated Acids. *J. Pharm. Sci.* **1973**, *62*, 154–158. [[CrossRef](#)]
26. Ma, Y.; Zhang, K.; Li, C.; Zhang, T.; Gao, N. Oxidation of Sulfonamides in Aqueous Solution by UV-TiO₂-Fe(VI). *BioMed Res. Int.* **2015**, *2015*, 973942. [[CrossRef](#)]
27. Yadav, M.S.P.; Neghi, N.; Kumar, M.; Varghese, G.K. Photocatalytic-oxidation and photo-persulfate-oxidation of sulfadiazine in a laboratory-scale reactor: Analysis of catalyst support, oxidant dosage, removal-rate and degradation pathway. *J. Environ. Manag.* **2018**, *222*, 164–173. [[CrossRef](#)]
28. Ismail, L.; Rifai, A.; Ferronato, C.; Fine, L.; Jaber, F.; Chovelon, J.M. Towards a better understanding of the reactive species involved in the photocatalytic degradation of sulfaclozine. *Appl. Catal. B Environ.* **2016**, *185*, 88–99. [[CrossRef](#)]
29. Baran, W.; Adamek, E.; Sobczak, A.; Makowski, A. Photocatalytic degradation of sulfa drugs with TiO₂, Fe salts and TiO₂/FeCl₃ in aquatic environment—Kinetics and degradation pathway. *Appl. Catal. B Environ.* **2009**, *90*, 516–525. [[CrossRef](#)]
30. Nahar, S.; Hasegawa, K.; Kagaya, S.; Kuroda, S. Adsorption and aggregation of Fe(III)-hydroxy complexes during the photodegradation of phenol using the iron-added-TiO₂ combined system. *J. Hazard. Mater.* **2009**, *162*, 351–355. [[CrossRef](#)]
31. Adamek, E.; Baran, W.; Ziemiańska, J.; Sobczak, A. The Comparison of Photocatalytic Degradation and Decolorization Processes of Dyeing Effluents. *Int. J. Photoenergy* **2013**, *2013*, 578191. [[CrossRef](#)]
32. Kuburović, D.N.; Golubović, A.V.; Babinčev, L.M. Development of new smart metal nanomaterials based on titanium-dioxide for photocatalytic and antimicrobial activities. *Mil. Tech. Cour.* **2018**, *66*, 771–835. [[CrossRef](#)]
33. Lin, S.; Huang, H.; Ma, T.; Zhang, Y. Photocatalytic Oxygen Evolution from Water Splitting. *Adv. Sci.* **2021**, *8*, 2002458. [[CrossRef](#)]
34. Zhou, A.; Wang, Y.; Sun, S.; Xin, X.; Wang, M.; Zhao, Q.; Jia, R. Removal of sulfadiazine in a modified ultrafiltration membrane (PVDF-PVP-TiO₂-FeCl₃) filtration-photocatalysis system: Parameters optimizing and interferences of drinking water. *Environ. Sci. Pol. Res.* **2020**, *27*, 45605–45617. [[CrossRef](#)] [[PubMed](#)]
35. Feng, W.; Nansheng, D. Photochemistry of hydrolyticiron (III) species and photoinduced degradation of organic compounds. *Chemosphere* **2000**, *41*, 1137–1147. [[CrossRef](#)]
36. Mills, A.; O'Rourke, C.; Moore, K. Powder semiconductor photocatalysis in aqueous solution: An overview of kinetics-based reaction mechanisms. *J. Photochem. Photobiol. A Chem.* **2015**, *310*, 66–105. [[CrossRef](#)]

37. Fox, M.A.; Dulay, M.T. Heterogeneous Photocatalysis. *Chem. Rev.* **1993**, *93*, 341–357. [CrossRef]
38. Yang, H.; Li, G.; An, T.; Gao, Y.; Fu, J. Photocatalytic degradation kinetics and mechanism of environmental pharmaceuticals in aqueous suspension of TiO₂: A case of sulfa drugs. *Catal. Today* **2010**, *153*, 200–207. [CrossRef]
39. Curcó, D.; Giménez, J.; Addardak, A.; Cervera-March, S.; Esplugas, S. Effects of radiation absorption and catalyst concentration on the photocatalytic degradation of pollutants. *Catal. Today* **2002**, *76*, 177–188. [CrossRef]
40. González, A.S.; Martínez, S.S. Study of the sonophotocatalytic degradation of basic blue 9 industrial textile dye over slurry titanium dioxide and influencing factors. *Ultrason. Sonochem.* **2008**, *15*, 1038–1042. [CrossRef]
41. Chen, C.Y. Photocatalytic degradation of azo dye reactive orange 16 by TiO₂. *Water Air Soil Pollut.* **2009**, *202*, 335–342. [CrossRef]
42. Carp, O.; Huisman, C.L.; Reller, A. Photoinduced reactivity of titanium dioxide. *Prog. Solid State Chem.* **2004**, *32*, 33–177. [CrossRef]
43. Kiwi, J.; Lopez, A.; Nadtochenko, V. Mechanism and Kinetics of the OH-Radical Intervention during Fenton Oxidation in the Presence of a Significant Amount of Radical Scavenger (Cl⁻). *Environ. Sci. Technol.* **2000**, *34*, 2162–2168. [CrossRef]
44. Schneider, J.T.; Firak, D.S.; Ribeiro, R.R.; Peralta-Zamora, P.G. Use of scavenger agents in heterogeneous photocatalysis: Truths, half-truths, and misinterpretations. *Phys. Chem. Chem. Phys.* **2020**, *22*, 15723–15733. [CrossRef]
45. Zhang, K.; Parker, K.M. Halogen radical oxidants in natural and engineered aquatic systems. *Environ. Sci. Technol.* **2018**, *52*, 9579–9594. [CrossRef]
46. Prajapat, G.; Rathore, U.; Gupta, R.; Bhojak, N. Thermal and biological evolution of Fe(III)-Sulfanilamide complexes synthesized by green strategy. *AIP Conf. Proc.* **2018**, *1953*, 080025.
47. Pervaiz, M.; Riaz, A.; Munir, A.; Saeed, Z.; Hussain, S.; Rashid, A.; Adnan, A. Synthesis and characterization of sulfonamide metal complexes as antimicrobial agents. *J. Mol. Struct.* **2020**, *1202*, 127284. [CrossRef]
48. Chen, J.; Stepanovic, S.; Draksharapu, A.; Gruden, M.; Browne, W.R. A Non-Heme Iron Photocatalyst for Light-Driven Aerobic Oxidation of Methanol. *Angew. Chem. Int. Ed.* **2018**, *57*, 3207–3211. [CrossRef]
49. Litter, M.I.; Slodowicz, M. An overview on heterogeneous Fenton and photo Fenton reactions using zero valent iron materials. *J. Adv. Oxid. Technol.* **2017**, *20*. [CrossRef]
50. Li, X.; Li, J.; Bai, J.; Dong, Y.; Li, L.; Zhou, B. The Inhibition Effect of Tert-Butyl Alcohol on the TiO₂ Nano Assays Photoelectrocatalytic Degradation of Different Organics and Its Mechanism. *Nano-Micro Lett.* **2016**, *8*, 221–231. [CrossRef]
51. Thompson, T.L.; Yates, J.T. TiO₂-based Photocatalysis: Surface Defects Oxygen and Charge Transfer. *Top. Catal.* **2005**, *35*, 197–210. [CrossRef]
52. Louwse, M.J.; Baerends, E.J. Oxidative properties of FeO²⁺: Electronic structure and solvation effects. *Phys. Chem. Chem. Phys.* **2006**, *9*, 156–166. [CrossRef] [PubMed]
53. Baran, W.; Adamek, E.; Sobczak, A.; Sochacka, J. The comparison of photocatalytic activity of Fe-salts, TiO₂ and TiO₂/FeCl₃ during the sulfanilamide degradation process. *Catal. Commun.* **2009**, *10*, 811–814. [CrossRef]
54. Luo, T.; Wan, J.; Ma, Y.; Wang, Y.; Wan, Y.J. Sulfamethoxazole degradation by an Fe(II)-activated persulfate process: Insight into the reactive sites, product identification and degradation pathways. *Environ. Sci. Process. Impacts* **2019**, *21*, 1560–1569. [CrossRef] [PubMed]
55. Liu, L.; Lin, S.; Zhang, W.; Farooq, U.; Shen, G.; Hu, S. Kinetic and mechanistic investigations of the degradation of sulfachloropyridazine in heat-activated persulfate oxidation process. *Chem. Eng. J.* **2018**, *346*, 515–524. [CrossRef]
56. Ji, Y.; Fan, Y.; Liu, K.; Kong, D.; Lu, J. Thermo activated persulfate oxidation of antibiotic sulfamethoxazole and structurally related compounds. *Water Res.* **2015**, *87*, 1–9. [CrossRef] [PubMed]
57. Inczedy, J. *Analytical Applications of Complex Equilibria*; Ellis Horwood Ltd.: New York, NY, USA, 1976.
58. Fittschen, C.; Hippler, H.; Viskolcz, B. The β C–C bond scission in alkoxy radicals: Thermal unimolecular decomposition of t-butoxy radicals. *Phys. Chem. Chem. Phys.* **2000**, *2*, 1677–1683. [CrossRef]
59. Reza, K.M.; Kurny, A.; Gulshan, F. Parameters affecting the photocatalytic degradation of dyes using TiO₂: A review. *Appl. Water Sci.* **2015**, *7*, 1569–1578. [CrossRef]
60. Tombácz, E. pH-dependent surface charging of metal oxides. *Period. Polytech. Chem. Eng.* **2009**, *53*, 77–86. [CrossRef]
61. Uhlemann, T.; Seidel, S.; Müller, C.W. Site-specific binding of a water molecule to the sulfa drugs sulfamethoxazole and sulfisoxazole: A laser-desorption isomer-specific UV and IR study. *Phys. Chem. Chem. Phys.* **2018**, *20*, 6891–6904. [CrossRef]
62. ISO. ISO 9887:1992(E) *Water Quality—Evaluation of the Aerobic Biodegradability of Organic Compounds in an Aqueous Medium—Semi-Continuous Activated Sludge Method (SCAS)*; International Organization for Standardization: Geneva, Switzerland, 1992.
63. U.S. Pharmacopeia. Available online: http://www.pharmacopeia.cn/v29240/usp29nf24s0_m79120.html (accessed on 18 July 2021).
64. Selleckchem. Available online: <https://file.selleckchem.com/downloads/struct/gentamicin-sulfate-chemical-structure-s4030.gif> (accessed on 18 July 2021).
65. Pubchem. Available online: <https://pubchem.ncbi.nlm.nih.gov/> (accessed on 18 July 2021).
66. Qiang, Z.; Adams, C. Potentiometric determination of acid dissociation constants (pKa) for human and veterinary antibiotics. *Water Res.* **2004**, *38*, 2874–2890. [CrossRef] [PubMed]
67. Bielski, B.H.; Cabelli, D.E. Superoxide and Hydroxyl Radical Chemistry in Aqueous Solution. In *Active Oxygen in Chemistry*; Foote, C.S., Valentine, J.S., Greenberg, A., Liebman, J.F., Eds.; Structure Energetics and Reactivity in Chemistry Series; Springer: Berlin/Heidelberg, Germany, 1995.
68. Crowell, R.A.; Lian, R.; Sauer, M.C., Jr.; Oulianov, D.A.; Shkrob, I.A. Geminate recombination of hydroxyl radicals generated in 200 nm photodissociation of aqueous hydrogen peroxide. *Chem. Phys. Lett.* **2004**, *383*, 481–485. [CrossRef]

69. Amor, C.; Marchão, L.; Lucas, M.S.; Peres, J.A. Application of advanced oxidation processes for the treatment of recalcitrant agro-industrial wastewater: A review. *Water* **2019**, *11*, 205. [CrossRef]
70. Mailloux, R.J. Teaching the fundamentals of electron transfer reactions in mitochondria and the production and detection of reactive oxygen species. *Redox Biol.* **2015**, *4*, 381–398. [CrossRef] [PubMed]
71. Collin, F. Chemical basis of reactive oxygen species reactivity and involvement in neurodegenerative diseases. *Int. J. Mol. Sci.* **2019**, *20*, 2407. [CrossRef] [PubMed]
72. Duesterberg, C.K.; Mylon, S.E.; Waite, T.D. pH effects on iron-catalyzed oxidation using Fenton's reagent. *Environ. Sci. Technol.* **2008**, *42*, 8522–8527. [CrossRef]
73. Burbano, A.A.; Dionysiou, D.D.; Suidan, M.T.; Richardson, T.L. Oxidation kinetics and effect of pH on the degradation of MTBE with Fenton reagent. *Water Res.* **2005**, *39*, 107–118. [CrossRef]
74. Sági, G.; Csay, T.; Szabó, L.; Pátzay, G.; Csonka, E.; Takács, E.; Wojnárovits, L. Analytical approaches to the OH radical induced degradation of sulfonamide antibiotics in dilute aqueous solutions. *J. Pharm. Biomed. Anal.* **2015**, *106*, 52–60. [CrossRef]
75. Bach, A.; Shemer, H.; Semiat, R. Kinetics of phenol mineralization by Fenton-like oxidation. *Desalination* **2010**, *264*, 188–192. [CrossRef]
76. Mezyk, S.P.; Neubauer, T.J.; Cooper, W.J.; Peller, J.R. Free-radical-induced oxidative and reductive degradation of sulfa drugs in water: Absolute kinetics and efficiencies of hydroxyl radical and hydrated electron reactions. *J. Phys. Chem. A* **2007**, *111*, 9019–9024. [CrossRef]
77. Cheng, S.; Zhang, X.; Yang, X.; Shang, C.; Song, W.; Fang, J.; Pan, Y. The multiple role of bromide ion in PPCPs degradation under UV/chlorine treatment. *Environ. Sci. Technol.* **2018**, *52*, 1806–1816. [CrossRef] [PubMed]
78. Osfor, M.M.; Kensarah, O.; Azzeh, F.; Elmadbouly, M.A.; El-Qutry, M. Biochemical changes in lipid and carbohydrate metabolism in obese diabetic male albino rats. *Int. J. Nutr. Food. Sci.* **2013**, *2*, 24–30. [CrossRef]
79. Lee, J.; Von Gunten, U.; Kim, J.H. Persulfate-based advanced oxidation: Critical assessment of opportunities and roadblocks. *Environ. Sci. Technol.* **2020**, *54*, 3064–3081. [CrossRef] [PubMed]
80. Kwon, B.G.; Kim, J.O.; Kwon, J.K. An Advanced Kinetic Method for HO₂/O₂[−] Determination by Using Terephthalate in the Aqueous Solution. *Environ. Eng. Res.* **2012**, *17*, 205–210. [CrossRef]
81. Abbas, A.A.; Jingsong, G.; Ping, L.Z.; Ya, P.Y.; Al-Rekabi, W.S. Review on Landfill leachate treatments. *J. Appl. Sci. Res.* **2009**, *5*, 534–545.
82. Yu, X.Y.; Bao, Z.C.; Barker, J.R. Free radical reactions involving Cl[•], Cl₂^{−•}, and SO₄^{−•} in the 248 nm photolysis of aqueous solutions containing S₂O₈^{2−} and Cl. *J. Phys. Chem. A* **2004**, *108*, 295–308. [CrossRef]
83. Friedmann, D.; Hakki, A.; Kim, H.; Choi, W.; Bahnemann, D. Heterogeneous photocatalytic organic synthesis: State-of-the-art and future perspectives. *Green Chem.* **2016**, *18*, 5391–5411. [CrossRef]
84. Pagsberg, P.; Munk, J.; Anastasi, C.; Simpson, V.J. Reaction of hydroxymethyl radicals with oxygen, nitric oxide, and nitrogen dioxide at room temperature. *J. Phys. Chem.* **1989**, *93*, 5162–5165. [CrossRef]
85. Ross, A.B.; Neta, P.; Ross, A.B.; Neta, P. *Rate Constants for Reactions of Aliphatic Carbon-Centered Radicals in Aqueous Solution*; (No. NSRDS-NBS-70); Notre Dame University Press: Notre Dame, IN, USA, 1982. Available online: <https://www.nist.gov/system/files/documents/srd/NSRDS-NBS-70-2.pdf> (accessed on 19 July 2021).
86. Wayner, D.D.M.; Houmam, A. Redox properties of free radicals. *Acta Chem. Scand.* **1998**, *52*, 377–384. [CrossRef]
87. Wardman, P. Reduction potentials of one-electron couples involving free radicals in aqueous solution. *J. Phys. Chem. Ref. Data* **1989**, *18*, 1637–1755. [CrossRef]
88. Denisov, E.T.; Denisova, T.G.; Pokidova, T.S. *Handbook of Free Radical Initiators*; John Wiley & Sons: Hoboken, NJ, USA, 2005.
89. Standard Electrode Potential (Data Page). Available online: https://en.wikipedia.org/wiki/Standard_electrode_potential (accessed on 19 July 2021).
90. Rajagopalan, R.; Chen, B.; Zhang, Z.; Wu, X.L.; Du, Y.; Huang, Y.; Zhang, H. Improved reversibility of Fe³⁺/Fe⁴⁺ redox couple in sodium super ion conductor type Na₃Fe₂(PO₄)₃ for sodium-ion batteries. *Adv. Mater.* **2017**, *29*, 1605694. [CrossRef] [PubMed]